JOURNAL
ENGINEERING MECHANICS DIVISION
Proceedings of the American Society of Civil Engineers

CONTENTS

April, 1956

Papers

JOURNAL
ENGINEERING MECHANICS DIVISION
Proceedings of the American Society of Civil Engineers

INELASTIC BUCKLING OF NON-UNIFORM COLUMNS

John E. Goldberg,[1] M. ASCE, John L. Bogdanoff,[2] and Hsu Lo[3]
(Proc. Paper 943)

SYNOPSIS

A numerical procedure is presented for calculating the critical loads of non-uniform pin-ended columns in the elastic or inelastic range. The procedure is based upon transformation of the differential equation to an integral equation which is solved numerically for trial values of the critical load.

If an initially straight pin-ended column is subjected to a slowly increasing axial load, the column will buckle when the load exceeds the value of P corresponding to the first eigenvalue of the following differential equation together with appropriate boundary conditions:

$$E_t I \frac{d^2y}{dx^2} + Py = 0$$

$$\text{or} \quad \frac{d^2y}{dx^2} = -\frac{Py}{E_t I} \tag{1}$$

where $E_t = E_t(x,P)$ = tangent modulus

$I = I(x)$ = moment of inertia of cross section

P = axial load

x = longitudinal coordinate

y = lateral deflection

Also L = length of column.

Note: Discussion open until September 1, 1956. Paper 943 is part of the copyrighted Journal of the Engineering Mechanics Division of the American Society of Civil Engineers, Vol. 82, No. EM 2, April, 1956.

1. Associate Prof. of Structural Eng., Purdue Univ., Lafayette, Ind.
2. Prof. of Eng. Science, Purdue Univ., Lafayette, Ind.
3. Prof. of Aeronautical Eng., Purdue Univ., Lafayette, Ind.

The above equation merely states that in some particular configuration, $y = y(x)$, which is arbitrarily small, the column is in a state of equilibrium when the applied load has been increased slowly to the critical load. Taking the internal bending moment as

$$M = -E_t I \frac{d^2y}{dx^2} \tag{2}$$

and equating this expression to the applied moment, P times y, leads to (1).

For the case of the pin-ended column, the boundary conditions may be taken as

$$y(0) = 0 \tag{3a}$$

$$y(L) = 0 \tag{3b}$$

or, alternatively, since the bending moment vanishes at the ends of the column,

$$\frac{d^2y(0)}{dx^2} = 0 \tag{3c}$$

$$\frac{d^2y(L)}{dx^2} = 0 \tag{3d}$$

It is convenient to rewrite the above equations in terms of a non-dimensional independent variable

$$s = \frac{x}{L} \tag{4}$$

and it is easily seen that

$$\frac{d^2y}{dx^2} = \frac{1}{L^2} \frac{d^2y}{ds^2} \tag{4a}$$

Consequently, the use of (4) and (4a) in (1) results in the equation,

$$\frac{d^2y}{ds^2} = -\frac{PL^2}{E_t I} y \tag{5}$$

with boundary conditions

$$y(0) = 0 \tag{5a}$$

$$y(1) = 0 \tag{5b}$$

or, alternatively,

$$\frac{d^2y(0)}{ds^2} = 0 \tag{5c}$$

$$\frac{d^2y(1)}{ds^2} = 0 \tag{5d}$$

Equation (5) is readily transformed to an integral equation by the following device. We substitute for the second derivative of y a new dependent variable Y(s), so that

$$\frac{d^2y}{ds^2} = Y(s) \tag{6a}$$

$$\frac{dy}{ds} = \int_0^s Y(\xi)\, d\xi - C_1 \tag{6b}$$

$$y = \int_0^s (s-\xi) Y(\xi) d\xi - C_1 s - C_2 \tag{6c}$$

We observe that the last of (6) and the boundary condition (5a) at s = 0 require that

$$C_2 = 0$$

The substitution of (6) into (5) therefore yields the following Volterra integral equation of the second kind,

$$Y(s) = \frac{PL^2}{E_t I}\left[-s\int_0^s Y(\xi) d\xi + \int_0^s \xi Y(\xi) d\xi + C_1 s\right] \tag{7}$$

while the boundary condition at s = 1 becomes

$$Y(1) = 0 \tag{7a}$$

By (7) it is found that Y(0) = 0 which, of course, agrees with (5c).

A solution of (7), linear in C_1, can be found by numerical methods described below for any value of P. The values of P associated with solutions satisfying the boundary condition, (7a), represent estimates of critical loads corresponding to the various modes of buckling of the column. The lowest of these P's greater than zero is the critical load of the column.

In terms of C_1 and for a given value of P, (7) represents an initial value problem for which an approximate solution may be found by the following method. We divide the range of integration (0,1) into n equal segments with boundary and division points located at $s_0, s_1, s_2, \ldots\ldots, s_{n-1}, s_n$. The points s_0 and s_n correspond to the ends of the column. The length of each

segment is b = 1/n. At the j-th division point Y(s) takes on the approximate value Y_j. Between division points, an interpolation of $Y(\xi)$ is used, thus permitting evaluation of the sectionalized integrals of (7). If the column is divided into a sufficient number of segments, the assumption that $Y(\xi)$ varies linearly over each segment will give good results.

Assuming linear variation over each segment, the approximate form of $Y(\xi)$ for integration in (7) takes on the polygonal character indicated in Fig. 1. With this assumption, it is easily seen that

$$\int_0^{s_j} Y(\xi)\,d\xi = b\frac{Y_0}{2} + bY_1 + \ldots + bY_{j-1} + b\frac{Y_j}{2}$$

$$= b\left[\frac{Y_0}{2} + \sum_1^{j-1} Y_k + \frac{Y_j}{2}\right]$$

and

$$\int_0^{s_j} Y(\xi)\,d\xi = \frac{b}{3}\frac{Y_0 b}{2} + bY_1 b + 2bY_2 b + \ldots\ldots + (j-1)bY_{j-1}b + (j-\tfrac{1}{3})b\frac{Y_j b}{2}$$

$$= b^2\left[\frac{Y_0}{6} + \sum_1^{j-1} kY_k + (\frac{j}{2} - \tfrac{1}{6})Y_j\right] \qquad (8)$$

Substituting (8) into (7), collecting terms in Y_j, and making use of the fact that $Y_0 = 0$ leads to

$$Y_j\left[1 + \frac{PL^2b^2}{6E_tI}\right] = C_1 j\frac{PL^2b}{E_tI} - \frac{PL^2b^2}{E_tI}\left[j\sum_1^{j-1} Y_k - \sum_1^{j-1} kY_k\right]$$

which may be written as

$$Y_j\left[\frac{n^2E_tI}{PL^2} + \frac{1}{6}\right] = C_1 jn - j\sum_1^{j-1} Y_k + \sum_1^{j-1} kY_k \qquad (9)$$

If the summations in (9) are transposed to the left-hand side, it is seen that the solution must be linear in C_1. Consequently, for the present purposes, it suffices to select any convenient value for C_1, say unity.

Suggested Procedure

The following procedure is suggested for the determination of the critical load of a non-uniform column. The procedure is essentially a trial-and-error method.

1) Divide the column into n equal segments and tabulate area, A, and moment of inertia, I, at each division point and at the terminal point.

2) Select a trial value of the axial load.

3) Compute the average stress at each division point and at the terminal point, and determine the tangent modulus for each point at the applied

stress. The tangent modulus may be determined from a tangent modulus curve or from a stress-strain curve, or it may be determined by means of an analytical expression for the stress-strain curve.

4) Using the following formula,

$$Y_j = \frac{jn - j\sum_{1}^{j-1} Y_k + \sum_{1}^{j-1} kY_k}{\frac{n^2 E_t I}{PL^2} + \frac{1}{6}} \tag{9a}$$

compute Y_j at $j = 1, 2, \ldots, n$. This may be done by desk computing methods or by digital computer.

5) If Y_n is found to be zero, then the trial load which has been used is a critical load. It is the critical load corresponding to the lowest mode of buckling if Y_j has the same algebraic sign throughout.

6) If Y_n is not zero (or approximately so), a new trial value of P should be selected and steps 2 to 5 repeated. If Y changes sign before the end point, n, is reached, this implies that a point of inflection or a hinge exists within the column and, therefore, the previous trial load is the critical load for a shorter column. Consequently, for the next trial, a lesser value of P should be used. Conversely, if Y does not change sign within the column, this corresponds to buckling of a somewhat longer column and, consequently, a larger value of P should be selected for the next trial.

It is, of course, unlikely that the boundary condition at s_n will be satisfied by the first trial. Since a second trial will be necessary, it is desirable to use the results of the previous calculation as a guide in selecting a new trial value of the axial load. By interpolation or extrapolation, the approximate point at which Y becomes zero may be found. If the point at which Y becomes zero is close to the end of the column, an estimate of the correction to the trial value of the critical load may be obtained by the following device. Let Δs be the distance of this inflection point from s_n, being positive if the inflection point is found to lie beyond the end of the column, and negative if it is found to lie within the column. Then the correction, ΔP, to the previous trial value, P_1, may be taken as

$$\Delta P = 2P_1 \Delta s \tag{10}$$

and the value to be used as a second trial may be taken as

$$P_2 = P_1(1 + 2\Delta s) \tag{11}$$

Equation (10) is obtained by differentiating the Euler formula with respect to the length, assuming that the average tangent modulus will not change greatly. Thus

$$P_1 = \frac{\pi^2 E_t I}{L^2} \tag{12}$$

where the bars over E_t and I indicate properties having the character of averages, then

$$\Delta P = -\frac{2\pi^2 \bar{E}_t \bar{I}}{L^3} \Delta L \approx -\frac{\Delta L}{L}$$

or

$$\Delta P = 2P_1 \Delta s \qquad (13)$$

If the additional terms which enter into the total differential of (12) can be computed readily, i.e., the terms involving the differentials of the tangent modulus and the moment of inertia, a more refined expression for the correction to the previous trial value may be obtained. However, it is doubtful whether, under ordinary circumstances, too much effort at this point is justified since the final result probably will be obtained by interpolation. Since (10) is not in general the total differential of (12), this equation should be used only as a means of estimating a correction. The final result is best obtained by interpolation or extrapolation from trial results which are reasonably well converged.

A variation of (9) is sometimes convenient for computation. For this purpose, let the product E_tI at some station, say s_0, be selected as a reference value and designated $(E_tI)_0$. Also let

$$\frac{E_t I}{(E_t I)_0} = r(s,p)$$

and let

$$\frac{\pi^2 (E_t I)_0}{PL^2} = \frac{1}{p}$$

The latter represents that ratio of Euler load of a uniform bar having the section properties of the reference station to the trial load. Then (9) may be written

$$Y_j \left[\frac{n^2 r}{p\pi^2} + \frac{1}{6}\right] = C_1 jn - j \sum_1^{j-1} Y_k + \sum_1^{j-1} kY_k \qquad (9b)$$

Examples and Results

Example 1. Uniform Bar in Elastic Range

This example is included merely to establish the potentialities of the method with respect to accuracy. The problem was worked using 5, 10, and 20 intervals. For a uniform bar, r_j in (9b) is always equal to unity. As discussed above, C_1 is taken as unity.

In each case, a first trial value was taken as five percent greater than the Euler load; hence $p_1 = 1.05$. Second trials were made with $p_2 = 0.95$. In each case, correction formula (13) was also applied to obtain a value which could be taken, if desired, for a subsequent trial. Linear interpolation or extrapolation was used to determine Δs, realizing, of course, that this is increasingly

inaccurate as n decreases and that a second order difference expansion should be used for better results. Starting with p_2 for n_5 and using extrapolation based upon second differences to compute Δs gives a corrected p of 1.018 instead of 1.0472 as shown for linear extrapolation.

An alternative procedure which consists merely of interpolating between p_1 and p_2 to find the value of p at which Y_n vanishes was also used. These interpolated values were taken as a third trial value and the calculations were repeated, leading to the results shown in the last table.

Example 2. Column with Linearly Varying Thickness

A 1"-wide solid column having a thickness varying linearly from 1" to 0.5" and a length of 10" is considered. Values of the tangent modulus are taken from Fig. 2. Calculations are made following the scheme given in Table II, with n = 10.

A first trial was made using P = 50,000 lbs. and gave $Y_n = -1.603$ as compared with a maximum Y equal to 7.48. This indicates that the trial value of P was too large. Using a rough graph of the values of Y_8, Y_9, and Y_n in lieu of an interpolation formula, the point of inflection was found to be about one-tenth of one segment above the bottom, hence Δs may be taken as -0.01, and by (13), $\Delta P = 2(50{,}000)(-0.01) = -1000$ lbs. It is realized, however, that the apparent precision is misleading. Nevertheless, the indicated correction was applied and the process repeated with P = 49,000 lbs. The calculations are shown in Table II.

It is seen that, for P = 49,000 lbs., $Y_n = 0.488$. Interpolating between this result and the result for P = 50,000 lbs. gives a final critical load of 49,233 lbs.

CONCLUSION

Numerous methods exist for transforming equation (7) into a set of linear algebraic equations. In the foregoing, linear interpolation has been used over each segment. This has led to a simple formula, (9), for constructing a set of algebraic equations whose coefficients form a triangular matrix, and hence these equations are easily solved. It may be observed that if a greater number of stations is taken in order to improve accuracy, which may be justified particularly for irregular columns, the labor increases only proportionately and not as a higher power of the order of the matrix.

In lieu of the linear interpolation which has been employed, it is clearly possible to use parabolic, cubic, or higher order interpolation formulas. This would require the simultaneous solution, by pairs in the case of the parabolic formula, by threes in the case of the cubic formula, and so on, of the final equations. An alternative procedure which retains the triangular nature of the system of equations and yet provides generally improved accuracy may be obtained by using single-step forward-integration based upon any desired degree of polynomial. Ultimately, one may construct an interpolating polynomial of the Lagrange type which covers all division points on the column. Such methods tend to lose the computational simplicity of equation (9), and it is perhaps preferable to use the linear method with a larger number of stations if greater accuracy is desired.

The method which has been presented may be extended to the case of

columns with one or more abrupt changes in section. Different arbitrary constants of integration will exist for each portion, but relations between them are obtained from the continuity conditions at each step.

BIBLIOGRAPHY

1. "Application of Volterra Linear Integral Equations to the Numerical Solution of Beam Vibration Problems" by J. L. Bogdanoff, J. E. Goldberg, and Hsu Lo, Proc. First Midwestern Conference on Solid Mechanics, Urbana, Illinois, April 1953, pp. 81-88.

2. "An Integral Equation Approach to the Problem of Approximating to the Torsional Natural Frequencies and Modes of a Bar" by J. L. Bogdanoff, J. E. Goldberg, and Hsu Lo, unpublished, December 1952.

3. "Theory of Measurement of Wind by Shooting Spheres Upwards" by L. F. Richardson, Phil. Trans of Royal Soc. London, Series A., Vol. 223, Sept. 1923, pp. 345-382.

4. "On the Numerical Solution of Volterra Integral Equations" by Carl Wagner, Journal of Math. and Physics, 32, 4, pp. 289-301, Jan. 1954.

5. "Application of Volterra Linear Integral Equation to the Numerical Solution of Vibration Problems - II" by J. L. Bogdanoff, J. E. Goldberg, and Hsu Lo, Journal of the Aeronautical Sciences, Vol. 21, No. 6 (June, 1954) pp. 383-389.

TABLE I

Example 1

FIRST TRIALS, VARIOUS n's, p = 1.05

n	Max Y	Y_n	Y_{n-1}	Δs	Δp	p
20	.16	-.01193	.01395	-.0231	-.0485	1.0015
10	.16	-.01031	.04104	-.0201	-.0422	1.0078
5	.16	-.00401	.09368	-.0082	-.0172	1.0328

SECOND TRIALS, VARIOUS n's, p = 0.95

n	Max Y	Y_n	Y_{n-1}	Δs	Δp	p
20	.15	.01263	.03576	.0273	.0573	1.0073
10	.15	.01403	.05935	.0309	.0649	1.0144
5	.15	.01946	.10358	.0463	.0972	1.0472

ALTERNATE INTERPOLATION PROCEDURE AND RESULTS OF THIRD TRIALS

n	Y_n for p_1	Y_n for p_2	Interp.p for Y_n=0	Y_n for Interp.p
20	-.01193	.01263	1.00143	.00016
10	-.01031	.01403	1.0076	.00016
5	-.00401	.01946	1.033	.00008

TABLE II
Example 2

First Trial: n = 10, P = 50,000 lbs., $n^2/PL^2 = 1/50{,}000$

(1)	(2)	(3)	(4)	(5)	(6)	(7)	(8)	(9)	(10)	(11)	(12)	(13)	(14)	(15)	(16)
j	jn	A	I	$\frac{P}{A}$ $\frac{P}{(3)}$	E_t Fig.2	$\frac{n^2 E_t I}{PL^2}$	(7)+1/6	$\sum_1^{j-1} Y_k$ (15) from prev. row	$\sum_1^{j-1} kY_k$ (16) from prev. row	$j\sum_1^{j-1} Y_k$ (1)x(9)	(2) + (10) - (11)	Y_j (12)/(8)	jY_j (1)x(13)	$\sum_1^{j} Y_k$ (9)+(13)	$\sum_1^{j} kY_k$ (10)+(14)
1	10	.95	.07145	52.6	25.0	35.70	35.87	0	0	0	10	.279	.279	.279	.279
2	20	.90	.06075	55.5	23.9	29.00	29.17	.279	.279	.558	19.721	.677	1.354	.956	1.633
3	30	.85	.05118	58.8	22.5	23.10	23.27	.956	1.633	2.868	28.765	1.235	3.705	2.191	5.338
4	40	.80	.04267	62.5	21.0	17.90	18.07	2.191	5.338	8.764	36.574	2.025	8.100	4.216	13.438
5	50	.75	.03516	66.7	19.3	13.58	13.75	4.216	13.438	21.080	42.358	3.080	15.400	7.296	28.838
6	60	.70	.02858	71.4	17.4	9.94	10.11	7.296	28.838	43.776	45.062	4.460	26.760	11.756	55.598
7	70	.65	.02289	76.9	15.2	6.96	7.13	11.756	55.598	82.292	43.306	6.074	42.518	17.830	98.116
8	80	.60	.01800	83.4	12.7	4.57	4.74	17.830	98.116	142.640	35.476	7.484	59.872	25.314	157.988
9	90	.55	.01386	90.9	9.6	2.66	2.83	25.314	157.988	227.826	20.162	7.124	64.116	32.438	222.104
10	100	.50	.01042	100.0	6.0	1.25	1.42	32.438	222.104	324.380	-2.276	-1.603			

Second Trial: n = 10, P = 49,000 lbs., $n^2/PL^2 = 1/49{,}000$

1	10	.95	.07145	51.6	25.3	36.85	37.02	0	0	0	10	.270	.270	.270	.270
2	20	.90	.06075	54.4	24.2	30.04	30.21	.270	.270	.540	19.730	.653	1.306	.923	1.576
3	30	.85	.05118	57.7	22.9	23.90	24.07	.923	1.576	2.769	28.807	1.197	3.591	2.120	5.167
4	40	.80	.04267	61.3	21.5	18.75	18.92	2.120	5.167	8.480	36.687	1.939	7.756	4.059	12.923
5	50	.75	.03516	65.4	19.8	14.20	14.37	4.059	12.923	20.295	42.628	2.966	14.830	7.025	27.753
6	60	.70	.02858	70.0	18.0	10.49	10.66	7.025	27.753	42.150	45.603	4.278	25.668	11.303	53.421
7	70	.65	.02289	75.4	15.8	7.38	7.55	11.303	53.421	79.121	44.300	5.868	41.076	17.171	94.497
8	80	.60	.01800	81.7	13.3	4.89	5.06	17.171	94.497	137.368	37.129	7.338	58.704	24.509	153.201
9	90	.55	.01386	89.1	10.3	2.92	3.09	24.509	153.201	220.581	22.620	7.320	65.880	31.829	219.081
10	100	.50	.01042	98.0	6.8	1.45	1.62	31.829	219.081	318.290	.791	.488			

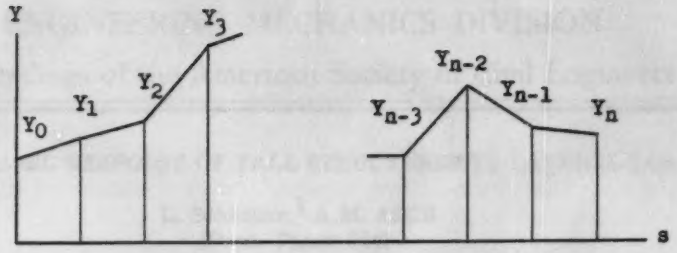

FIG. 1. POLYGONAL APPROXIMATION FOR Y(s).

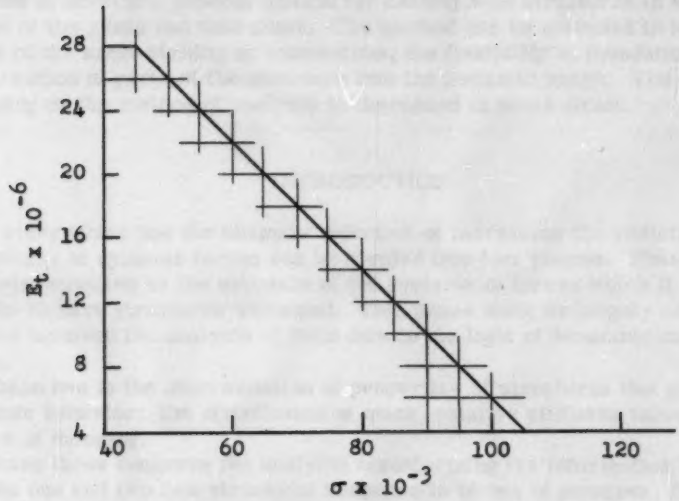

FIG. 2. TANGENT MODULUS CURVE FOR EXAMPLE 2.

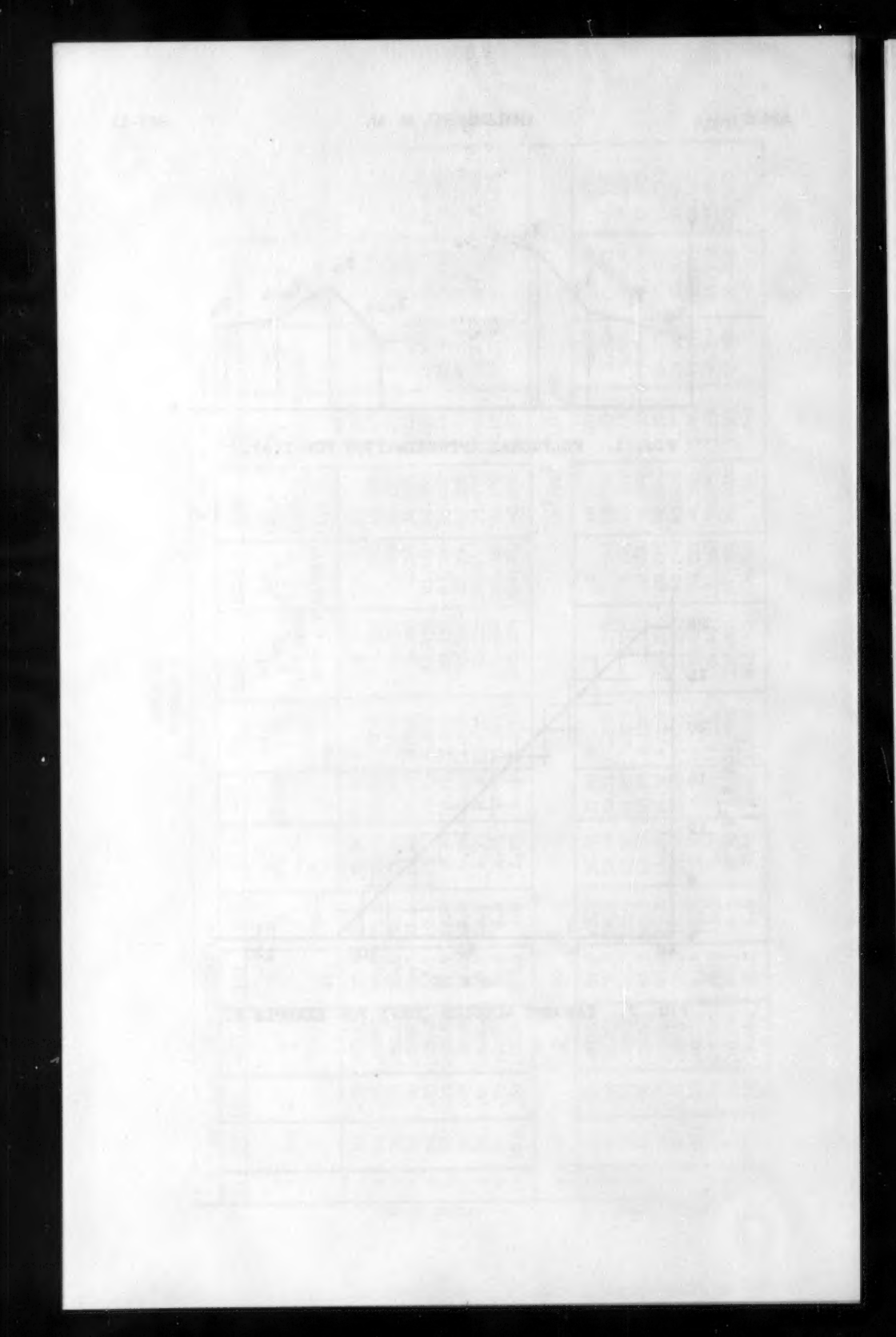

JOURNAL
ENGINEERING MECHANICS DIVISION
Proceedings of the American Society of Civil Engineers

THE DYNAMIC RESPONSE OF TALL STRUCTURES TO LATERAL LOADS

L. Schenker,[1] A.M. ASCE
(Proc. Paper 944)

ABSTRACT

The paper deals with some aspects of the analytical procedures for computing the response of structures to dynamic forces. It is restricted to the consideration of tall structures, such as tier buildings and chimneys, subjected to lateral forces or displacements. The concept of "stiffness matrix" is used to develop a general method for dealing with structures in which rotation of the joints can take place. The method can be extended to take account of the semi-rigidity of connections, the flexibility of foundations and deformation of parts of the structure into the inelastic range. The effect of damping on the method of analysis is discussed in some detail.

INTRODUCTION

A study which has the ultimate objective of increasing the resistance of structures to dynamic forces can be divided into four phases. Phase one is the determination or the estimate of the systems of forces which it is practicable to have structures withstand. This phase must be largely experimental and involves the analysis of field data in the light of economic considerations.

Phase two is the determination of properties of structures that govern dynamic behavior: the distribution of mass, relative stiffness values and the nature of damping.

Phase three concerns the analysis transforming the information from phases one and two into structural response in terms of stresses, deflections, moments and shears.

Since the analytical procedures of phase three are bound to be complex and time consuming there is a need for simplification leading to procedures suitable for design purposes. This can be considered the fourth phase.

Note: Discussion open until September 1, 1956. Paper 944 is part of the copyrighted Journal of the Engineering Mechanics Division of the American Society of Civil Engineers, Vol. 82, No. EM 2, April, 1956.

1. Member of Technical Staff, Bell Telephone Labs., Inc., Murray Hill, N. J.

This paper deals with some aspects of phase three, the analytical procedures for computing the response of structures to dynamic forces. It is restricted to the consideration of tall structures, i.e. tier buildings, chimneys and towers, subject to lateral forces or displacements. The effect of a number of factors, usually neglected in the dynamic analysis of structures, is discussed.

Elastic Structures Without Damping

The following assumptions are made in this study:

i) The mass of a structure can be represented by a number of discrete masses concentrated at various stations.

ii) The external forces are considered to be concentrated at the stations.

It is frequently assumed in the dynamic analysis of tall structures that the motion of any one story is resisted only by the spring forces brought into play by the relative displacement from the two neighboring stories. This implies that the sets of columns between floors act like simple springs connecting the masses of the floors, as shown in Fig. 1(a). This assumption is justified only if the girders are much more rigid than the columns, so that almost no rotation takes place at the joints. In the more general case, discussed in this paper, when the stiffness of the girders is of the same order as that of the columns, the motion of each floor is affected by the motion of every other floor. The model in Fig. 1(b) represents this state of affairs. Under this condition the equations of motion can no longer be set up by inspection.

For a given system of external lateral forces $F_r(t)$—(r refers to the stations)—the dynamic response of a structure can be calculated, provided that the numerical values of all masses M_r and the lateral stiffness matrix

$$[S] = \begin{bmatrix} S_{11} & S_{12} & S_{13} & \cdots & S_{1n} \\ S_{21} & S_{22} & S_{23} & \cdots & S_{2n} \\ S_{31} & S_{32} & S_{33} & \cdots & S_{3n} \\ \cdot & \cdot & \cdot & \cdots & \cdot \\ \cdot & \cdot & \cdot & \cdots & \cdot \\ \cdot & \cdot & \cdot & \cdots & \cdot \\ S_{n1} & S_{n2} & S_{n3} & \cdots & S_{nn} \end{bmatrix} \tag{2.1}$$

are known. The lateral stiffness matrix for a structure with n masses is defined here as a square array of n^2 numbers, the r-th row of which represents the static forces that have to be applied at the various levels in order to produce a unit displacement at the r-th level, but a zero displacement at all other levels.

The importance of the concept of the stiffness matrix [S] is that it is a

static property of the structure. Yet, apart from the data on the masses, it is all the information that is required to compute the undamped response of a structure to any given system of lateral time-varying forces. The refinement with which [S] is computed or computable governs the accuracy of the final answer. For example, if [S] is computed, taking account of the rocking at the foundation, lengthening and shortening of columns, rotation of the joints, the answer is correspondingly characteristic. Furthermore, it is feasible to determine [S] experimentally.

The equations describing the undamped motion which results from the application of a system of forces F_r are:

$$[M]\{\ddot{x}\} + [S]\{x\} = \{F\} \tag{2.2}$$

where [M] is the diagonal matrix representing the mass at every station. Salvadori[1]* has shown that these simultaneous differential equations can be solved conveniently by the transformation

$$x(t) = \sum_{j=1}^{j=n} \varphi_{rj} q_j(t) \tag{2.3}$$

where ϕ_{rj} is the normalized shape of the j-th mode, corresponding to the natural (circular) frequency ω_j. The generalized coordinates q_j are determined from the solution of the n uncoupled differential equations

$$\ddot{q}_j + \omega_j^2 q_j = Q_j \tag{2.4}$$

where $Q_j = \sum_{r=1}^{r=n} \varphi_{rj} F_r$ are the generalized forces corresponding to q_j.

If the functions $F_r(t)$ and hence $Q_j(t)$ are so irregular that they cannot be expressed in mathematical form, equations (2.4) can be solved by Newmark's numerical method.[2]

The Stiffness and Flexibility Matrices

Consideration is given here to a multi-story, multi-bay framed structure, with girders that are not infinitely rigid, so that joint rotation can take place. It is assumed that the structure has a rigid foundation and that the lateral movements resulting from the length changes in the columns can be neglected.

In Fig. 2 a three-story structure of this type is shown schematically. Bearing in mind the definition of the stiffness matrix, it is required to find a square array of nine numbers, each row of which represents the forces at the three levels, compatible with a unit deflection at one level and zero deflection at the other two. Moment-distribution is ideally suited to the computation of these forces. In Fig. 2 the applied force S_{22} and the two out-of-balance forces S_{21} and S_{23} form the second row of the stiffness matrix for the structure

* This and subsequent raised numerals in parentheses refer to the list of references at the end of the paper.

shown. Only three simple moment distributions have to be carried out for the determination of the complete matrix

$$[S] = \begin{bmatrix} S_{11} & S_{12} & S_{13} \\ S_{21} & S_{22} & S_{23} \\ S_{31} & S_{32} & S_{33} \end{bmatrix} \tag{3.1}$$

When [S] has been determined and M is known equations of the type (2.2) can be written down and solved. This procedure is applicable also to frames with semi-rigid connections, provided that for the determination of [S] the moment-distribution for semi-rigid frames is used.(3)

When the effect of the flexibility of the foundation and "beam action" of the whole structure—i.e. length changes in the columns—are to be taken into account, it is convenient to work in terms of the flexibility matrix rather than the stiffness matrix. The former is the reciprocal of the stiffness matrix. Stiffness matrices cannot be added by adding algebraically the corresponding terms, but this can be done with flexibility matrices. Denoting the flexibility matrices due to shear action, beam action of the whole structure and due to base rotation by [f'], [f''], [f'''], respectively, the total flexibility matrix [f] is given by

$$[f] = [f'] + [f''] + [f'''] \tag{3.2}$$

Some Numerical Examples

The response of the structure shown in Fig. 3(a) to the forces as shown in Fig. 3(b) will now be determined according to several alternative assumptions.

Although it is indicated in Fig. 3(a) that the moment of inertia of all girders is 1675 in.^{4} the calculations are first carried out on the assumption that the girders are infinitely rigid. Moreover, length changes in the columns are ignored, as is the flexibility of the foundation. The stiffness matrix for this condition is readily computed. The shear K_r that must be applied between floors to produce a unit relative displacement is

$$K_r = \frac{48EI_r}{h_r^3}$$

where I_r is the moment of inertia of each of the four columns. Below the r-th floor and h_r is the distance between floors. Thus

$$K_1 = 166{,}000 \text{ lb. in.}^{-1}; \quad K_2 = K_3 = 234{,}000 \text{ lb. in.}^{-1}$$

from which

$$[S] = \begin{bmatrix} 400 & -234 & 0 \\ -234 & 468 & -234 \\ 0 & -234 & 234 \end{bmatrix} 10^3 \text{ lb. in.}^{-1} \qquad (4.1)$$

and the equations of motion, after dividing both sides by 1000, are:

$$\begin{aligned} 0.832\ddot{x}_1 + 400x_1 - 234x_2 &= 52(1 - 0.8t) \\ 0.832\ddot{x}_2 - 234x_1 + 468x_2 - 234x_3 &= 52(1 - 0.8t) \\ 0.416\ddot{x}_3 - 234x_2 + 234x_3 &= 26(1 - 0.8t) \end{aligned} \qquad (4.2)$$

The solutions of (4.2) are obtainable by the method outlined in section 2. The natural circular frequencies are found to be 7.74 sec.$^{-1}$, 22.56 sec.$^{-1}$ and 32.20 sec.$^{-1}$ and the mode shapes in normalized form are:

$$\begin{aligned} &\text{1st mode:} \quad \varphi_{11} = 0.0160 \quad \varphi_{21} = 0.0241 \quad \varphi_{31} = 0.0271 \\ &\text{2nd mode:} \quad \varphi_{12} = -0.0279 \quad \varphi_{22} = 0.0027 \quad \varphi_{32} = 0.0288 \\ &\text{3rd mode:} \quad \varphi_{13} = 0.0124 \quad \varphi_{23} = -0.0248 \quad \varphi_{33} = 0.0295 \end{aligned} \qquad (4.3)$$

The uncoupled equations of motion, corresponding to (2.4) are

$$\begin{aligned} \ddot{q}_1 + 59.9q_1 &= 2790(1 - 0.8t) \\ \ddot{q}_2 + 508.5q_2 &= -561(1 - 0.8t) \\ \ddot{q}_3 + 1036.5q_3 &= 122(1 - 0.8t) \end{aligned} \qquad (4.4)$$

and the complete solution is

$$\begin{aligned} x_1 &= 0.0160q_1 - 0.0279q_2 + 0.0124q_3 \\ x_2 &= 0.0241q_1 + 0.0027q_2 - 0.0248q_3 \\ x_3 &= 0.0271q_1 + 0.0288q_2 + 0.0295q_3 \end{aligned} \qquad (4.5)$$

where

$$\begin{aligned} q_1 &= 46.57[1 + 1.005 \sin(7.74t - 1.468) - 0.8t] \\ q_2 &= -1.10[1 + \sin(22.56t - 1.536) - 0.8t] \\ q_3 &= 0.12[1 + \sin(32.20t - 1.546) - 0.8t] \end{aligned} \qquad (4.6)$$

The error introduced by the assumption that the girders are infinitely rigid is now examined. It is necessary to compute a revised stiffness matrix allowing for the fact that the moments of inertia of the girders are as indicated in Fig. 3(a). Using moment distribution, the revised stiffness matrix is computed to be

$$[S] = \begin{bmatrix} 372 & -227 & 24 \\ -227 & 378 & -175 \\ 24 & -175 & 153 \end{bmatrix} 10^3 \text{ lb. in.}^{-1} \qquad (4.7)$$

indicating some reduction in stiffness, as is to be expected. From here on, the procedure for analyzing the structure is the same as in the previous example. Equations of motion, corresponding to (4.2) can be written down and solved. The natural frequencies are somewhat lower: 6.57, 19.25, and 28.73 radians per second. The revised mode shapes are:

$$\begin{array}{lllll} \text{1st mode:} & \varphi_{11} = 0.0144 & \varphi_{21} = 0.0241 & \varphi_{31} = 0.0287 \\ \text{2nd mode:} & \varphi_{12} = -0.0260 & \varphi_{22} = -0.0038 & \varphi_{32} = 0.0320 \\ \text{3rd mode:} & \varphi_{13} = 0.0179 & \varphi_{23} = -0.0245 & \varphi_{33} = 0.0236 \end{array} \qquad (4.8)$$

These values should be compared with (4.3). The complete solutions are not written down explicitly, but can be obtained as before.

Behavior in the Inelastic Range

The dynamic behavior of systems which become inelastic after certain critical deflections are exceeded can be treated by methods which are basically the same as those used for perfectly elastic systems. A step-by-step procedure can be used, re-writing the equations of motion when the stiffness matrix changes as a result of yielding in some part of the structure. When the stage is reached that unrestrained deformation can take place, a procedure developed by Salvadori and Bleich[4] may be used. It will be found that in this last stage the lowest natural frequency is zero. The appropriate mode shapes can be computed as usual.

The Effect of Damping

The main purpose of this section is to emphasize the difficulties that are encountered in analyzing the response of a multi-degree-of-freedom structure, if account is to be taken of the effect of damping. To facilitate mathematical manipulations it is customary to assume that damping is viscous, i.e. that the damping forces are proportional to the rate of change of displacements. For a single-degree-of-freedom system there is then no further difficulty. In a multi-degree-of-freedom system a new problem arises: is damping a function of the absolute or relative velocities of stations or of both? Even if the degree of damping is known or has been assumed—say, 10%

of critical damping—what are the values to be used for the damping coefficients C in the equations

$$M_r\ddot{x}_r + C_{r1}\dot{x}_1 + C_{r2}\dot{x}_2 + \ldots + C_{rn}\dot{x}_n + S_{r1}x_1 + S_{r2}x_2 + \ldots + S_{rn}x_n = F_r(t) \qquad (6.1)$$

The answer, in part, is that in many cases it is not necessary to know the values of the coefficients C, provided the percentages of critical damping in each mode are known. The procedure then is to solve the equations of motion (6.1), neglecting damping, as a first approximation. The effect of damping can be introduced subsequently into the uncoupled equations of motion of the type (2.4), one of which is associated with each mode. These uncoupled equations, with damping, have the form

$$\ddot{q}_j + 2\varepsilon_j\dot{q}_j + \omega_j^2 q_j = Q_j \qquad (6.2)$$

As an example, for damping in the first, second and third modes of 10%, 15% and 20% respectively, $\epsilon_1 = 0.1\,\omega_1$, $\epsilon_2 = 0.15\,\omega_2$, $\epsilon_3 = 0.2\,\omega_3$. Having solved (6.2) for the q_j the actual displacements x_r are again found from (2.3). For the assumption that the total damping effect is the sum of the damping effects associated with the various modes, the mode shapes ϕ are not modified by damping.

In some applications it is desirable, however, to be able to determine the numerical values of the coefficients C in equations (6.1). This is the case, for example, when the equations are to be solved directly by means of an analog computer. The problem, then, is to find the relationship between the coefficients C—of which there are n^2 in number—and the critical damping coefficients ϵ_j—of which there are n. This may be done as follows. The homogeneous part of the uncoupled equations of motion is

$$\ddot{q}_j + 2\varepsilon_j\dot{q}_j + \omega_j^2 q_j = 0, \quad (j = 1,2,\ldots n) \qquad (6.3)$$

of which the solution is

$$q_j = e^{-\varepsilon_j t}(B_j \cos \omega_j t + D_j \sin \omega_j t) \qquad (6.4)$$

The origin of time can be chosen so that at $t = 0$ all $x_r = 0$. Then the values of $\dot{x}_r$ at this time can be denoted by $\dot{x}_{ro}$. From (2.3) and the orthogonality condition for the mode shapes

$$\sum_{r=1}^{r=n} M_r\varphi_{rj}\varphi_{rk} = \begin{cases} 0, & \text{when } j \neq k \\ 1, & \text{when } j = k \end{cases}$$

it is found that

$$q_j = \sum_{r=1}^{r=n} M_r x_r \varphi_{rj} \tag{6.5}$$

Therefore the values of q_j at t = 0 are zero and all B_j in (6.4) are zero also. Hence

$$q_j = D_j e^{-\epsilon_j t} \sin \omega_j t \tag{6.6}$$

The equations of motion with damping can be written

$$[M][\varphi] \left\{\ddot{q}\right\} + [C][\varphi] \left\{\dot{q}\right\} + [S][\varphi] \left\{q\right\} = \left\{0\right\} \tag{6.7}$$

These must hold at t = 0, when $q_{jo} = 0$, $\dot{q}_{jo} = D_j\omega_j$ and $\ddot{q}_{jo} = -2D_j\epsilon_j\omega_j$. Therefore, at t = 0, (6.7) reads

$$[M][\varphi] \left\{-2D\epsilon\omega\right\} + [C][\varphi] \left\{D\omega\right\} = \left\{0\right\} \tag{6.8}$$

When (6.8) is expanded it may be seen that each of the n equations contains terms associated with all modes. Since it is feasible that an initial displacement may be imparted to the structure that will excite only one mode, the equations resulting from (6.11) must be true for any mode, one at the time. Hence

$$[M][\varphi][2D\epsilon\omega] = [C][\varphi][D\omega] \tag{6.9}$$

where $[2D\epsilon\omega]$ and $[D\omega]$ are diagonal matrices. It is thus permissible to cancel $D\omega$ on both sides. Consequently,

$$2[M][\varphi][\varepsilon] = [C][\varphi] \tag{6.10}$$

where

$$\varepsilon = \begin{bmatrix} \varepsilon_1 & 0 & 0 & \cdots & 0 \\ 0 & \varepsilon_2 & 0 & \cdots & 0 \\ \cdot & \cdot & \cdot & \cdots & \cdot \\ 0 & 0 & 0 & \cdots & \varepsilon_n \end{bmatrix} \tag{6.11}$$

(6.10) are n^2 equations in which the coefficients C are the only unknowns. In expanded form, for n = 3

$$C_{11}\varphi_{11} + C_{12}\varphi_{21} + C_{13}\varphi_{31} = 2\epsilon_1 M_1\varphi_{11}$$

$$C_{11}\varphi_{12} + C_{12}\varphi_{22} + C_{13}\varphi_{32} = 2\epsilon_2 M_1\varphi_{12} \qquad (6.12)$$

$$C_{11}\varphi_{13} + C_{12}\varphi_{23} + C_{13}\varphi_{33} = 2\epsilon_3 M_1\varphi_{13}$$

from which C_{11}, C_{12}, and C_{13} can be calculated. There are six more equations from which the other C's can be found. For the numerical example of section 4 of this paper, for 10% critical damping in all modes, $\epsilon_1 = 0.774$ sec.$^{-1}$, $\epsilon_2 = 2.256$ sec.$^{-1}$ and $\epsilon_3 = 3.220$ sec.$^{-1}$, so that

$$[C] = \begin{bmatrix} 3433 & -1210 & -198 \\ -1210 & 3385 & -1151 \\ -198 & -1151 & 1785 \end{bmatrix} \text{ sec.}^{-1} \qquad (6.13)$$

The equations of motion can now be set up in the form of (6.1) and solved with the analog computer.

CONCLUSION

As outlined in the Introduction, the approach to the solution of analysis and design problems involving structures subject to dynamic loads can be broken down into several phases. Of these, the present paper deals with methods of computing the response of tall structures to lateral dynamic loads. The emphasis is on some aspects of the problem which are often not taken into account, namely (i) joint rotation, (ii) deformation into the inelastic range, and (iii) damping. No suggestion is made at this time, as to whether these conditions will affect practical analysis and design procedures to any large extent. The contribution this paper is intended to make is to illustrate how the special aspects can be dealt with whenever necessary.

The procedure of setting up the equations of motion of a multi-degree-of-freedom system by making use of the concept of the stiffness matrix is frequently used in the aircraft structures field in one form or another. It might well be adopted by the civil engineer, because it throws a good deal of light on the dynamic behavior of a structure whose static properties are known.

The implications of the usual assumptions concerning damping in a multi-degree-of-freedom structure are often not fully appreciated. It is with this in mind that the discussion in section 6 of the paper was prepared.

This paper is based on parts of the author's doctoral dissertation which was developed under guidance of a committee under the chairmanship of Bruce G. Johnston, Professor of Structural Engineering, at the University of Michigan. Many helpful suggestions were made by Professor M. A. Brull, Department of Aeronautical Engineering, University of Michigan.

REFERENCES

1. "Earthquake Stresses in Shear Buildings," M. G. Salvadori, ASCE Proc. Separate No. 177, March 1953.

2. "Methods of Analysis for Structures Subjected to Dynamic Loading," N. M. Newmark, Directorate of Intelligence; H.Q. USAF, Washington, D. C., revised Dec. 1950.

3. "Analysis of Building Frames with Semi-Rigid Connections," B. G. Johnston, E. H. Mount, Trans. ASCE, Vol. 107, 1942.

4. "Impulsive Motion of Elasto-Plastic Beams," H. H. Bleich, M. G. Salvadori, ASCE Proc. Separate No. 287, Sept. 1953.

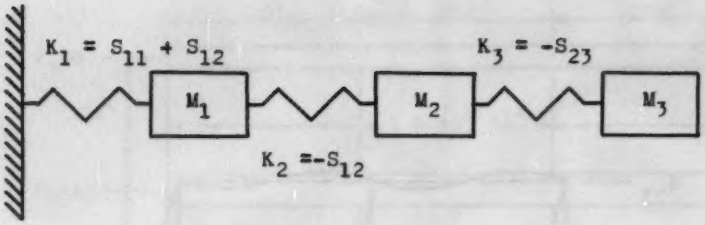

(a)

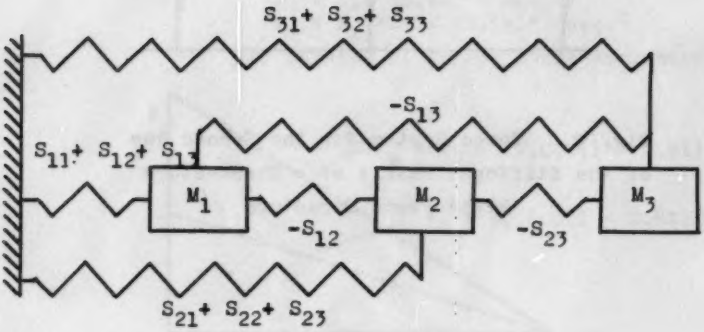

(b)

Fig. 1 Models of Simply and Multiply Connected Systems

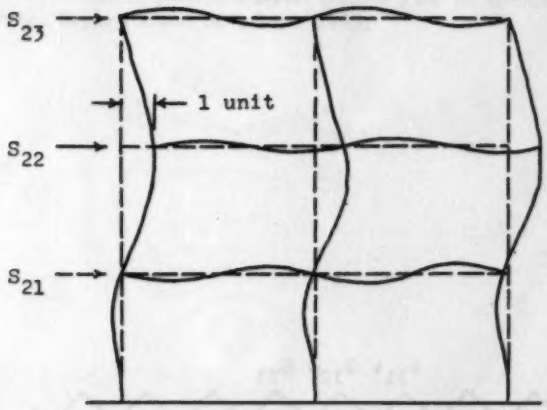

Fig. 2 Force System for the Second Row of the Stiffness Matrix of a Three-Story Rigid Frame Structure

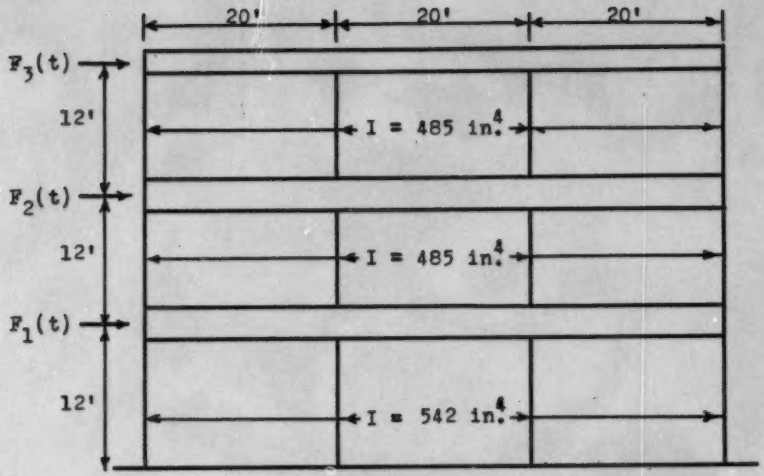

I for all girders 1675 in.^{4}
M_3 = 416 lb.in.$^{-1}$ sec.^{2}
$M_2 = M_1$ = 832 lb.in.$^{-1}$ sec.^{2}

(a) Details of Three- Story Structure

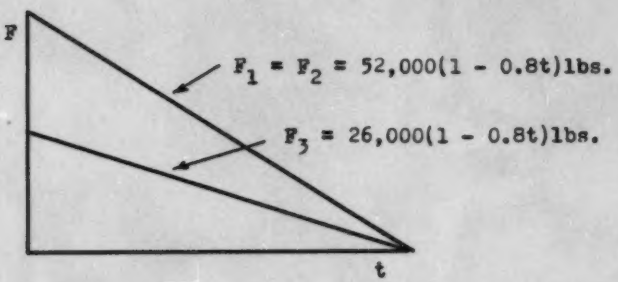

(b) Variation of External Forces

Fig. 3 Details of Three-Story Structure and Applied Forces

Paper 945 EM 2

JOURNAL
ENGINEERING MECHANICS DIVISION
Proceedings of the American Society of Civil Engineers

THE VISCOUS SUBLAYER ALONG A SMOOTH BOUNDARY

H. A. Einstein,* M. ASCE, and Huon Li
(Proc. Paper 945)

SYNOPSIS

If the sublayer is visualized as a steady, quasi-laminar flow, great difficulty is encountered in the physical description of the transition to the turbulent part of the flow. The proposed model visualizes a periodic growth and decay of the sublayer. The magnitude of the life-period of the sublayer can be predicted theoretically and has been checked by experiment. As a consequence of this model some predictions are made on the generation of turbulence near the boundary.

INTRODUCTION

The viscous sublayer in the sense of this derivation is a usually rather thin fluid layer along the smooth boundary of a turbulent fluid flow in which due to the proximity of the wall the turbulent pattern of flow can not develop freely. The presence of this layer under the given conditions is today admitted by all serious students of turbulence, but its exact physical description is not equally well agreed upon. The one point, where general agreement exists is the fact that at the boundary the entire shear stress is transmitted, in the fluid by viscosity, i.e., by molecular action. Outside the layer most of the shear is transmitted by eddy-viscosity or, in other words, by momentum exchange between fluid masses of larger than molecular size. But how the transition from molecular to molar units takes effect is not generally agreed upon, even if an ever-increasing amount of information becomes available from measurements in the proximity of frictional boundaries.

The engineering description of frictional effects in pipe and channel flow becomes most consistent if the assumption is made that turbulence is created at the frictional boundary.[1] This assumption is supported by the observation

Note: Discussion open until September 1, 1956. Paper 945 is part of the copyrighted Journal of the Engineering Mechanics Division of the American Society of Civil Engineers, Vol. 82, No. EM 2, April, 1956.

* Associate Prof., Mechanical Eng., Univ. of California, Berkeley, Calif.

1. Elevated numbers refer to corresponding numbers in the list of literature.

that turbulence is created only in connection with a frictional boundary or at the interface between fluid masses of different velocity. The latter is commonly found wherever separation occurs of a flow from a solid boundary, leaving a fluid body of different velocity between the main flow and the solid boundary. A good example for such a case is found along the wake of any submerged object, where the interface between main flow and wake is not stable, but steadily fluctuates, shedding constantly newly created eddies into the flow if the Reynolds Number is sufficiently high. The same process may also be observed at the wakes of the individual roughness elements of a hydraulically rough boundary. With the wakes located between the roughness elements, turbulence derived from a rough boundary can thus be said to originate at the wall, speaking from the viewpoint of the flow as a whole.

If the turbulence pattern and, particularly, the velocity distributions are compared which are derived from smooth boundaries with those along rough boundaries, the patterns are found to be identical, i.e., the equation of the time-average velocity distribution near a smooth boundary can be transformed into that near a rough boundary by mere replacement of the viscous length scale ν/u_* by a multiple of the roughness k_s, $(0.300\ k_s)$. This shows that there exists a basic similarity between the two processes. Particularly, it may be expected that also along the smooth boundary the turbulence must be created predominantly at the boundary itself, not somewhere in the free flow. A satisfactory model of the viscous sublayer must thus also explain how turbulence is created in this case. It is the purpose of this paper to show that a model can be found which describes the flow system along a smooth boundary on this basis and which is not contradicted by any available measurements.

A. The Proposed Model

To arrive at a workable model, let us imagine first that at a given instant the turbulent flow continues all the way to the boundary with a finite main velocity at the wall. The high velocity gradient at the wall calls for an extremely high viscous shear there which is not transmitted into the free fluid due to lack of velocity gradient farther away from the wall, but which decelerates the fluid adjacent to the boundary, creating a viscosity controlled layer or, to be consistent with common language, a viscosity controlled sub-layer, which grows with time in thickness. As the thickness of the sublayer grows, the boundary shear reduces and the growth becomes increasingly slower.

This sublayer is thus an unsteady laminar or near-laminar flow bounded on one side by the rigid wall, on the other side in a rather undetermined manner by the turbulent flow. It is comparable to a shear flow between two solid walls which have a constant velocity difference and which continuously increase their distance with fluid supplied constantly through the wall representing the turbulent fluid at a rate necessary to satisfy the continuity condition. It is easily visualized that the Reynolds Number of the sublayer continuously grows under these circumstances, indicating an ever-growing tendency to become unstable. It is to be expected under the steady effect of the disturbances from the turbulent flow outside that the sublayer flow will become unstable and turn into turbulence itself as soon as a critical Reynolds Number has been reached. Then turbulent mixing will occur between the previously turbulent flow and the newly created sublayer turbulence. With turbulent mixing much more effective than viscosity, it must be expected that the sublayer fluid is then accelerated by the turbulent outside fluid to about its own velocity in a

time much shorter than that which was required for the viscous build-up of the sublayer. After this the cycle is closed and a new cycle begins.

The inherently unsteady character of this flow is demonstrated by Fig. 1, in which two instantaneous views of flow conditions in a plastic transparent 2" diameter pipe are given. The discharge in both is 0.008 cfs, the average flow velocity 0.367 ft/sec., the Reynolds Number 5700, the Weisbach friction factor f = 0.036, the friction velocity $u_* = 0.0246$ ft/sec. and the sublayer thickness as commonly defined is:

$$\frac{11.6\,\nu}{u_*} = 5.1 \times 10^{-3} \text{ ft} \sim 1.5 \text{ mm}$$

A small hole was drilled into the bottom-wall of the pipe at about 6.0 cm of the scale permitting the injection of dye into the boundary sublayer. The dye was introduced at a very low constant rate and velocity. The dye should be expected not to mix with the turbulent flow if the viscous sublayer flow is steady. It is seen that in one photograph mixing occurs about 3 cm downstream—in the other almost immediately, indicating the existence of sporadic mixing as proposed in the unsteady sublayer model.

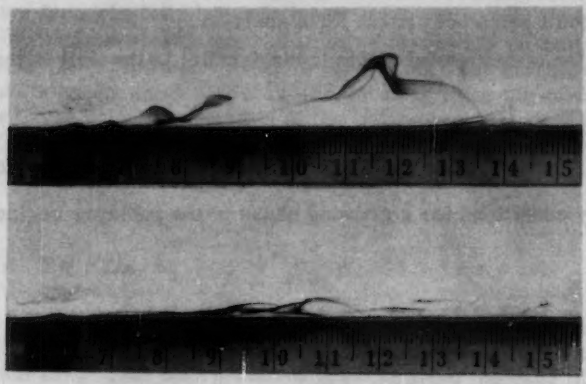

Fig. 1. Mixing of dye from the viscous sublayer of turbulent pipe flow into the main flow. Upper photograph shows almost immediate mixing from tube at cm 6, lower photograph shows delayed mixing, depending on phase of sublayer.

The above described cyclic growth and decay of the sublayer represents the fundamental idea on which the proposed model is based. Some modifications have been introduced, however, for the following mathematical description. First, the introduction of an imaginary outside boundary which permits the passage of fluid is actually not necessary since the distance to which viscous effects are felt regulates itself automatically if the depth of the turbulent flow is assumed to be large compared to the sublayer thickness. The displacement thickness of the sublayer may then be introduced as a measure for its thickness.

Secondly, in order to receive expressions which can be integrated and otherwise handled mathematically, the eddy-viscosity of the turbulent flow is assumed to be infinitely larger than the molecular viscosity of the fluid during the period of decay, resulting in a constant average velocity at all points of the turbulent flow. During the period of build-up the effect of eddy-viscosity is neglected.

Thirdly, it is assumed that the area of boundary over which simultaneous growth and decay of the sublayer occurs is in all directions large compared with the sublayer thickness, reducing the sublayer generation to a one-dimensional unsteady flow problem.

Introducing the following nomenclature, the generation of the sublayer can be described on the basis of the given three assumptions:

x, y, z	Cartesian coordinates.
z = 0	smooth boundary, flow at $z > 0$.
U, V, W	average velocity in turbulent flow, V = W = 0 at all points.
u, v, w	instantaneous sublayer velocities, v = w = 0.
U_o	representative velocity in turbulent range near the sublayer.
t	time.
T	total period of growth for a sublayer.

The equation of motion for a thin layer parallel to the wall is then

$$\frac{\partial u}{\partial t} = \nu \frac{\partial^2 u}{\partial z^2} \tag{1}$$

The boundary conditions for a growing phase of the sublayer beginning at t = 0 are

$$\begin{array}{llll} \text{for } t = 0 & & u = U_o & \text{for all } z > 0 \\ \text{for } t > 0 & \text{and} & z = 0 & u = 0 \\ \text{for } t > 0 & \text{and} & z \to \infty & u = U_o \end{array} \tag{2}$$

A solution for this flow is

$$u = \frac{2U_o}{\sqrt{\pi}} \int_0^H e^{-h^2}\, dh \tag{3}$$

with the parameter H defined as

$$H = \frac{z}{2\sqrt{\nu t}} \tag{4}$$

and h a variable of integration.

This solution, which is the Gaussian error integral, actually satisfies the boundary conditions (2) as can be seen very easily. For t = 0 the limit H becomes infinite and the integral

$$\frac{2}{\sqrt{\pi}} \int_0^{\infty} e^{-h^2} \, dh = 1 \qquad (5)$$

such that the first condition (2) is fulfilled. The same argument holds for $t > 0$ and $z = \infty$. For $z = 0$ and $t > 0$ the upper limit becomes $H = 0$ and with zero range of the integral of solution (3), the velocity u becomes zero, such that all boundary conditions are actually fulfilled.

The error integral can not be expressed algebraically in closed form, but has been tabulated and thus made available for numerical calculations.[2]

B. The Thickness Scale of the Sublayer

Equation (4) already indicates that the instantaneous boundary-sublayer thickness should be measured by a sliding scale, i.e., by the unit $\sqrt{\nu t}$, since all distances z from the boundary are measured by this unit. Let us try to understand the meaning of this unit. For this purpose the so-called "displacement thickness" of the boundary layer is calculated. The displacement thickness is the distance by which stream lines far away from the surface are diverted due to the velocity reduction of the incompressible fluid between the stream line and the boundary. The continuity equation for this flow indicates that the displacement thickness δ^* may be determined as

$$\delta^* = \int_0^{\infty} \left(1 - \frac{u}{U_o}\right) dz \qquad (6)$$

if an equal discharge is assumed to flow at all times between the boundary and the stream line. This interpretation is taken from the case of a boundary layer which is visualized as long, but not infinitely long, in which case the continuity may be established between a cross section 1 ahead of the boundary and section 2 through the boundary of Fig. 2.

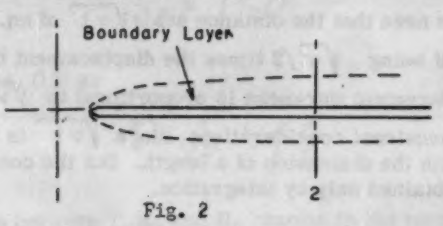

Fig. 2

Next, the value of δ^* is determined, introducing the value of u from eq. (3) into eq. (6)

$$\delta^* = \int_{z=0}^{\infty} \left(1 - \frac{2}{\sqrt{\pi}} \int_{h=0}^{H} e^{-h^2}\, dh\right) dz \qquad (7)$$

With the help of eq. (4) the distance z is now expressed in H, and eq. (5) is used to expand

$$\delta^* = 2\sqrt{\nu t} \int_{H=0}^{\infty} \left(\frac{2}{\sqrt{\pi}} \int_{h=0}^{\infty} e^{-h^2}\, dh - \frac{2}{\sqrt{\pi}} \int_{h=0}^{H} e^{-h^2}\, dh\right) dH$$

$$= 4\sqrt{\frac{\nu t}{\pi}} \int_{H=0}^{\infty} \left(\int_{h=H}^{\infty} e^{-h^2}\, dh\right) dH$$

Now the order of integrations is changed

$$\delta^* = 4\sqrt{\frac{\nu t}{\pi}} \int_{h=0}^{\infty} \left(\int_{H=0}^{h} e^{-h^2}\, dH\right) dh$$

which can once be integrated

$$\delta^* = 4\sqrt{\frac{\nu t}{\pi}} \int_{h=0}^{\infty} e^{-h^2}\, h\, dh$$

A second integration gives

$$\delta^* = 4\sqrt{\frac{\nu t}{\pi}}\, \frac{1}{2} = \frac{2}{\sqrt{\pi}} \sqrt{\nu t} \qquad (8)$$

From this may be seen that the distance scale $\sqrt{\nu t}$ of eq. (4) has physically the significance of being $\sqrt{\pi}/2$ times the displacement thickness. The result that the displacement thickness is proportional to $\sqrt{\nu t}$ could have been derived from dimensional considerations, since $\sqrt{\nu t}$ is the only parameter of the problem with the dimension of a length. But the constant of proportionality can be obtained only by integration.

C. The Shear Stress in the Sublayer

To become more familiar with the character of this flow, the shear stress may be calculated. As velocity gradients exist in the z-direction only one may write

$$\tau = \mu \frac{\partial u}{\partial z} = \mu \frac{U_0}{\sqrt{\pi \nu t}} e^{-\frac{z^2}{4\nu t}} \quad (9)$$

and at the boundary, where z = 0

$$\tau_0 = \mu \frac{U_0}{\sqrt{\pi \nu t}} \quad (10)$$

At time zero, when the turbulent flow with the constant velocity still reaches the boundary, the shear stress is infinite and subsequently reduces fast to ever-decreasing values. The significance of this infinite value may be tested by calculating its impulse or time integral. It may be agreed that an infinite instantaneous τ_0 - value may be acceptable in a physical problem as long as it has no lasting effect. The time integral is thus determined between time 0 and a final time T

$$\int_{t=0}^{T} \tau_0 \, dt = \int_{t=0}^{T} \mu \frac{U_0}{\sqrt{\pi \nu t}} \, dt = \frac{2 U_0 \rho}{\sqrt{\pi}} \sqrt{\nu T} \quad (11)$$

if the dynamic viscosity is expressed as $\mu = \nu \cdot \rho$ where ρ is the fluid density. It may very easily be seen from eq. (11) that the impulse for finite time intervals T is always finite and tends toward zero as T is reduced towards zero, indicating the insignificance of the high τ_0 at t = 0. From this the time average shear $\overline{\tau}_0$ may be calculated as

$$\overline{\tau}_0 = \frac{1}{T} \int_{T=0}^{T} \tau_0 \, dt = \frac{2 U_0 \rho}{\sqrt{\pi}} \sqrt{\frac{\nu}{T}} \quad (12)$$

and if common nomenclature is used which introduces the friction velocity u_* as

$$u_* = \sqrt{\overline{\tau}_0 / \rho} \quad (13)$$

one can rewrite eq. (12) as

$$u_*^2 = \frac{2}{\sqrt{\pi}} U_0 \sqrt{\frac{\nu}{T}}$$

and a relationship between T, u_* and U_0 results in the form

$$T = \frac{4}{\pi} \frac{U_0^2 \nu}{u_*^4} \quad (14)$$

This eq. (14) indicates that the growing period of the sublayer may be predicted under the assumed conditions from the kinematic viscosity of the fluid, the average flow and the shear velocities.

D. The Decay of the Sublayer

The decay process has been described already in general terms and the time necessary for the decay into turbulence and for the reacceleration of the sublayer fluid to the general flow velocity U_o outside the sublayer was assumed to be short compared with the build-up period T of the sublayer. Any values averaged during the build-up period may thus be assumed to represent averages for the total time.

The decay process itself is one of instability and is highly non-linear. At this time any mathematical description of the decay process itself appears to be utterly impossible. The condition of incipient instability, on the other hand, may be studied by a stability condition of the laminar sublayer flow. A dimensional consideration indicates that this condition is characterized by a critical Reynolds Number as in case of the corresponding laminar pipe or channel flow. If the Reynolds Number is introduced in the form

$$N_R^* = 4 \frac{\delta_T^* U_o}{\nu} \qquad (15)$$

it may be expected to correspond to the Reynolds Number for a pipe flow based on the pipe diameter. The use of the displacement thickness instead of the hydraulic radius may still change the resulting critical Reynolds Number from that of a pipe by a certain amount, and it is quite interesting to do some estimating of N_R^*. This can be done by estimating the velocity U_o for a given u_* from the main turbulent flow.

One may assume that U_o exists at a distance $z = n\delta_T^*$ from the boundary in the main turbulent flow. Then

$$\frac{U_o}{u_*} = 5.75 \log_{10} \left(9.05 \frac{n \delta_T^* u_*}{\nu} \right) \qquad (16)$$

If eqs. (14) and (8) are used to express δ_T^* in eq. (16), U_o/u_* may be determined as 12.39 for n = 1.0 and from that $N_R^* = 780$. Similarly, values of N_R^* can be obtained for other values of n as shown in Table 1.

TABLE 1

CRITICAL REYNOLDS NUMBERS FOR VARIOUS ASSUMPTIONS OF U_o

U_o at $y = 0.50\,\delta_T^*$	$N_R^* = 525$	$T = 131\,\nu/u_*^2$	$\delta_T^* = 12.90\,\nu/u_*$
U_o at $y = 1.0\,\delta_T^*$	$N_R^* = 780$	$T = 195\,\nu/u_*^2$	$\delta_T^* = 15.75\,\nu/u_*$
U_o at $y = 2\,\delta_T^*$	$N_R^* = 1073$	$T = 268\,\nu/u_*^2$	$\delta_T^* = 18.49\,\nu/u_*$
U_o at $y = 3\,\delta_T^*$	$N_R^* = 1256$	$T = 314\,\nu/u_*^2$	$\delta_T^* = 20.00\,\nu/u_*$

It is possible now to express all the variables of the problem in terms of this critical Reynolds Number as indicated in Table 1. The choice of the proper value for z/δ^*_T may be made only empirically from measurements, although one may conjecture that Table 1 covers the range within which the correct value may be found.

E. Momentum Transfer Through the Sublayer

Equations (8) and (12) can be combined into the form

$$\overline{\tau}_o = \rho U_o \frac{\delta^*_T}{T} \qquad (17)$$

which may be interpreted as a momentum equation. It indicates that the shear stress $\overline{\tau}_o$ which is transmitted from the wall to the sublayer per unit wall area is used totally to reduce 1/T times per second the velocity of a mass $\rho\ \delta_T{}^*$ from U_o to zero. An equal amount of momentum is transferred according to the same equation by the reacceleration of the same mass to U_o after it has become turbulent. This explanation and description of the momentum transfer from the sublayer to the turbulent flow is one of the great advantages of this model. It is clear that with this model not only momentum, but also fluid, dye, sediment, heat, etc. are transferred from the stream lined flow of the sublayer to the main turbulent flow at the end of each period T and from the turbulent flow to the sublayer during its build-up. Such transfer of matter has been observed and can not be explained with a basically steady flow pattern in the sublayer.

F. The Average Velocity Profile in the Sublayer

If the duration of the decay period is again assumed to be negligible with respect to the period of build-up, the average velocity distribution in the sublayer can be determined by averaging the velocity at a given distance z from the boundary over the build-up period T only. On the basis of eqs. (3) and (4) one can write

$$\frac{\overline{u}}{U_o} = \frac{2}{\sqrt{\pi}} \int_{t/T=0}^{1} \int_{h=0}^{z/2\sqrt{\nu T}} e^{-h^2}\, dh\ d\left(\frac{t}{T}\right) \qquad (18)$$

In this form eq. (18) shows that the proposed sublayer has a universally applicable velocity distribution if $\overline{u}/U_o$ is given in terms of $z/2\sqrt{\nu T}$. Herein are

$\overline{u}$ the time average sublayer velocity at a distance z from the boundary.

U_o the assumed to be constant turbulent velocity outside the sublayer.

ν the kinematic viscosity of the fluid.

T the period of the sublayer build-up.

This function of eq. (18) can not be integrated in closed form. Numerical integration gave the curve of Fig. 3 in the form of $\bar{u}/u_*$ against u_*z/ν.

G. The Root-Mean-Square (RMS) Deviation of the Instantaneous Sublayer Velocity From Its Average

The RMS value of the local velocity can also be determined numerically only. Its determination was based on the following transformation

$$\text{RMS} = \sqrt{\frac{1}{T}\int_0^T (u-\bar{u})^2\,dt} = \sqrt{\frac{1}{T}\int_0^T (u^2 - 2u\bar{u} + \bar{u}^2)\,dt}$$

$$= \sqrt{\frac{1}{T}\left\{\int_0^T u^2\,dt - 2\bar{u}\int_0^T u\,dt + \bar{u}^2\int_0^T dt\right\}}$$

$$= \sqrt{\frac{1}{T}\int_0^T u^2\,dt - \bar{u}^2} \qquad (19)$$

This expression can again be made dimensionless by division with u_* as is done in Fig. 4.

H. The Rate of Energy Dissipation in the Sublayer

It is very interesting to determine the percentage of the total flow energy which is dissipated into heat in the sublayer by viscous action and the remaining percentage which enters the main flow in the form of newly created turbulence. The rate of viscous energy dissipation can be directly calculated per unit time and volume

$$\phi = \mu\left(\frac{\partial u}{\partial z}\right)^2 \qquad (20)$$

The time average dissipation, again per unit of time and volume, is

$$\bar{\phi} = \mu\,\frac{1}{T}\int_0^T \left(\frac{\partial u}{\partial z}\right)^2 dt \qquad (21)$$

if $\mu\,\dfrac{\partial u}{\partial z}$ is taken from eq. (9)

$$\bar{\phi} = \frac{\mu}{T}\,\frac{U_0^2}{\pi\nu}\int_0^T \frac{1}{t}\,e^{\frac{-z^2}{2\nu t}}\,dt \qquad (22)$$

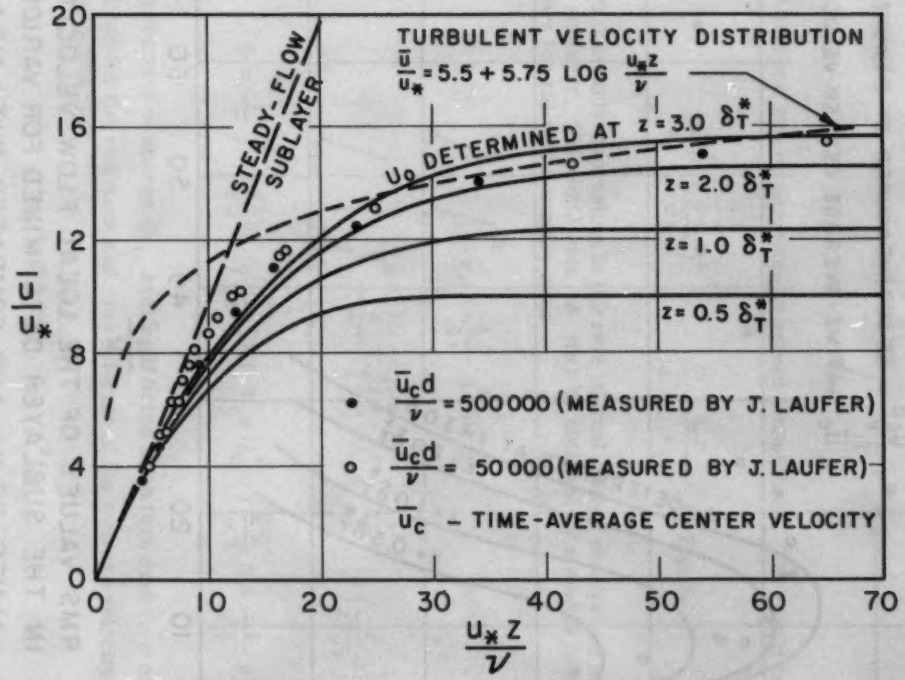

FIG. 3 TIME-AVERAGE VELOCITY DISTRIBUTIONS IN THE SUBLAYER FOR VARIOUS VALUES OF U_0 COMPARED WITH VALUES MEASURED BY LAUFER.

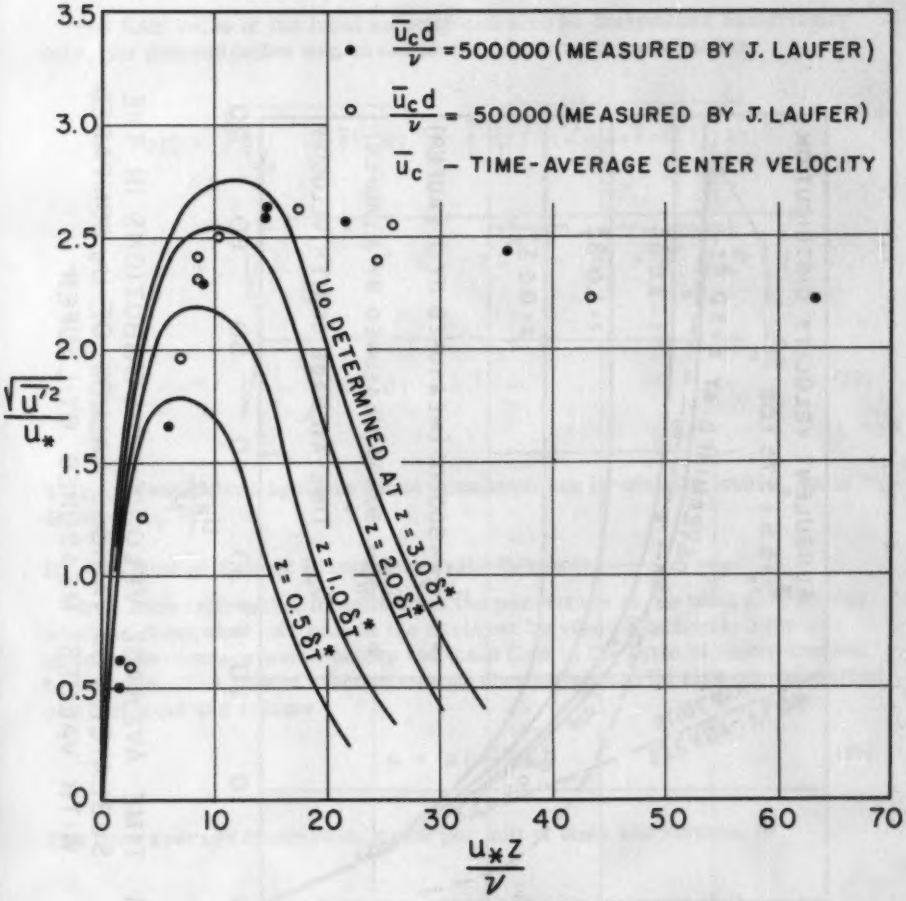

FIG. 4 RMS VALUES OF THE LOCAL FLOW VELOCITY IN THE SUBLAYER DETERMINED FOR VARIOUS VALUES OF U_o AND COMPARED WITH MEASUREMENTS BY J. LAUFER.

and with

$$S = - \frac{z^2}{2\nu t} \tag{23}$$

$$\bar{\phi} = - \frac{\rho U_0^2}{\pi T} \int_{-\infty}^{-z^2/2\nu T} \frac{1}{S} e^S \, dS \tag{24}$$

This integral can be numerically solved from tables. The result is given as a plot of

$$\frac{\nu^2}{u_*^4} \left(\frac{\overline{\partial u}}{\partial z} \right)^2 \quad \text{vs.} \quad \frac{u_* z}{\nu} \quad \text{in Fig. 5.}$$

Particularly interesting is the rate of total energy dissipation in the entire sublayer. This total rate Φ may be obtained by a double integration as follows for the unit boundary area

$$\Phi = \frac{1}{T} \int_{t=0}^{T} \int_{z=0}^{\infty} \nu \rho \left(\frac{\partial u}{\partial z} \right)^2 dz \, dt$$

$$= \frac{1}{T} \int_{t=0}^{T} \left[\int_{0}^{\infty} \frac{\rho}{\pi} \sqrt{\frac{2\nu}{t}} U_0^2 \, e^{-\frac{z^2}{2\nu t}} \, d\left(\frac{z}{\sqrt{2\nu t}} \right) \right] dt$$

$$\Phi = \frac{1}{T} \int_{t=0}^{T} \frac{\rho U_0^2}{\sqrt{\pi}} \sqrt{\frac{\nu}{2t}} \, dt = \rho U_0^2 \sqrt{\frac{2\nu}{\pi T}} = \rho \frac{U_0}{\sqrt{2}} u_*^2 \tag{25}$$

The total rate of energy Φ_t available in the main turbulent flow may be determined for the unit area and time in terms of the average velocity $U_{av.}$ of the turbulent flow

$$\Phi_t = \overline{\tau}_0 \, U_{av.} = \rho u_*^2 \, U_{av.} \tag{26}$$

from which the fraction of energy dissipation in the sublayer is

$$\frac{\Phi}{\Phi_t} = \frac{1}{\sqrt{2}} \frac{U_0}{U_{av.}} \tag{27}$$

I. Application of the Model to Actual Flows

In its application any such model must describe as many as possible of the various phases of the actual flow behavior. This model has the advantage over any quasi-steady-flow sublayer description, that is explains the exchange of matter between the turbulent flow and the boundary as it has been observed to exist (see Fig. 1). This is the great achievement of this approach.

No model and no theory are better, however, than the assumptions on which they are based. While it is believed that the basic description of the sublayer cycle is correct, some of the mathematical simplifications used in the derivation and solution of the equations are somewhat questionable. The assumption of an infinitely high eddy-viscosity and of the resulting constant flow velocity in the turbulent flow are definitely unrealistic. It will be necessary, therefore, to investigate the effect of this idealization of the flow. This can best be done by comparing actually observed velocity distributions with the prediction of the model. Fig. 3 shows a number of predicted velocity distributions based on various assumed U_o - values and corresponding experimental values measured by Laufer.[2] The measurement seems to confirm the contention that in a graph $(\bar{u}/u_*)$ against $(u_* z/\nu)$ the distribution is independent of the overall Reynolds Number of the flow. The graph indicates, furthermore, that the outside velocity U_o must probably be measured at a distance of between 2 and $3\delta_T^*$ to give a velocity distribution similar to the measured distribution.

Let us assume for the sake of discussion the value $z = 3.0\,\delta_T^*$ indicates the point of the turbulent velocity distribution curve (shown in Fig. 3 as dashed curve) where U_o is obtained. At this point $\bar{u}/u_* = 15.6$, indicated by the horizontal tangent to the calculated $\bar{u}/u_*$ - curve. It may be remembered now that due to the assumption of uniform turbulent velocity distribution the flow velocities in the range of the entire sublayer is assumed to have the value $\bar{u}/u_* = 15.6$ at the beginning of the viscous sublayer build-up period. This velocity distribution is assumed to have been created in the short preceding period of decay by turbulent momentum exchange with the outside turbulent flow. It would be more appropriate to assume that at the beginning of the viscous sublayer period the velocity distribution follows the extended turbulent velocity distribution. Unfortunately, this approach leads to hitherto unsurmountable mathematical difficulties. Also the physical picture becomes rather confused in that case, since then the transmission of momentum is simultaneously performed, partially by viscosity, partially by turbulence. All we may conclude with security at this time is that the proposed theory assumes at time zero near the boundary an excessively high flow velocity. With the time-average velocity nearly correct, the final minimum velocity is probably too low and it must be expected that the predicted RMS-values of the velocity near the boundary are too high.

Fig. 4 shows that this is actually so. Here the curves of the RMS-values of the sublayer velocity according to eq. (19) were plotted for various U_o-values and compared with values measured by Laufer. All curves are high along this steep rise from the wall as we have just predicted. They come to a sharp maximum near $(u_* z/\nu) = 6 - 12$ and then drop again reasonably sharp towards zero, while the measured values remain high for the rest of the section. This is perfectly reasonable, since the predicted curve describes the unsteady laminar flow only, while the measured points include in addition the fluctuations of the turbulence. Turbulence must be expected to reach its

maximum intensity just outside the sublayer, such that the difference of the predicted curves and the measured values is well explained for values of $(u_* z/\nu)$ larger than the maximum of the predicted RMS-curves.

From this comparison of measured and predicted values of velocity measurements, one must thus conclude that the proposed theory, though basically correct, gives only a rough approximation of the actual flow pattern.

This has a further consequence. The values for the predicted period T must also be expected to be larger than the actual values. This may easily be seen from the derivation of eq. (17). If the range of velocity change at various distances from the wall is effectively less than assumed, the number of changes per unit of time must be higher than predicted, to permit an equal shear to be transmitted by momentum exchange. Unfortunately, no measurements could be found in the literature from which the period T could be taken. There is not even mention that any periodicity of the process is indicated by available measurements.

The authors of this paper were so convinced of the superiority which the unsteady sublayer theory has over any quasi-steady description that they decided to attempt the experimental proof of its correctness.

J. The Basis of the Experimental Demonstration of the Periodic Character of the Sublayer

The fact that none of the successful investigators of sublayer flow in the past noticed any periodicity is sufficient proof that the periodicity can not be directly apparent in any velocity signal, but is probably concealed by large amplitude random disturbances originating in the turbulent flow outside the sublayer. It appeared thus to be most promising to locate the point of measurement as far away from the turbulent flow as possible, i.e., to measure at the frictional boundary itself. The flow velocity vanishes there and thus can not be measured. It must be expected, on the other hand, that the pressure reflects any such periodicity of the flow pattern. A pressure recording system was developed using a Rutishauser pressure gauge as described in Appendix I. But also this signal was expected to contain a large percentage of random noise created by the turbulence of the main flow, calling for a special method to detect any possible periodicity. The use of the available sound analyzers was soon dismissed as unreliable since their band width was excessive and their frequency range insufficient for low frequencies. Continuous records were thus made of the pressure and an auto-correlation curve constructed for the records. This method has the following value: Even if the major part of the signal fluctuations are irregular random fluctuations, this part of the signal will result in a regularly dropping correlation curve. If there is a periodic component added to the random signal, this part of the signal will appear as a superimposed periodic fluctuation in the correlation curve, too, as may be seen, for instance, in Fig. 6.

The auto-correlation coefficient for a continuous function of time such as the boundary pressure is

$$C = \frac{\int p_{(t)} \cdot p_{(t+\Delta t)}\, dt}{\sqrt{\int p^2_{(t)}\, dt}\sqrt{\int p^2_{(t+\Delta t)}\, dt}}$$

where $p_{(t)}$ is the pressure at time t, $p_{(t+\Delta t)}$ the same pressure at Δ t later

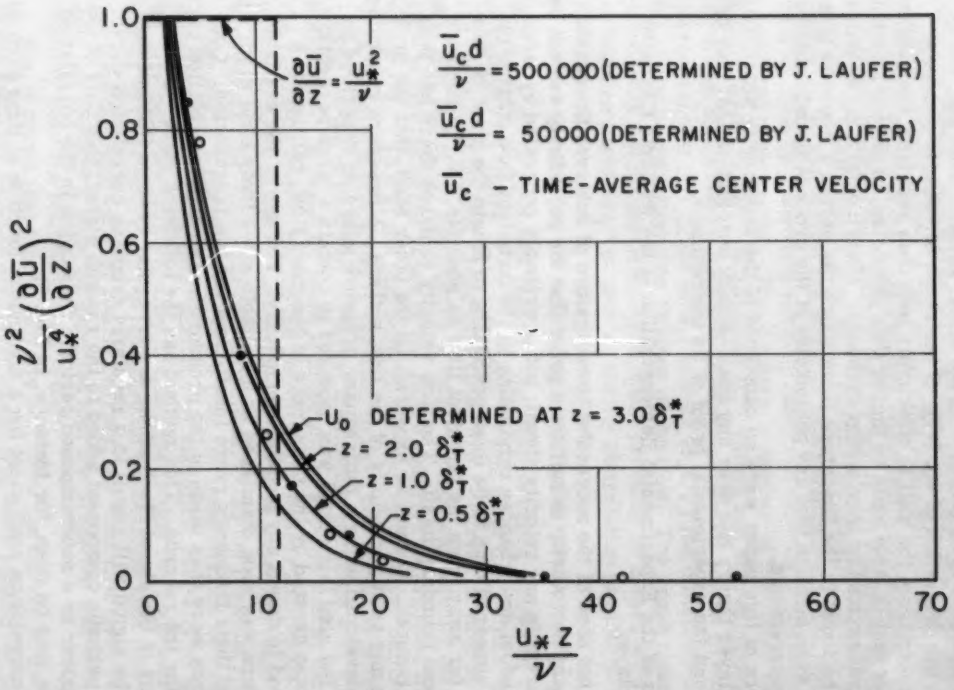

FIG. 5 DIRECT VISCOUS-DISSIPATION RATE IN THE SUB-LAYER DETERMINED FOR VARIOUS VALUES OF U_0 AND COMPARED WITH VALUES DETERMINED BY J. LAUFER.

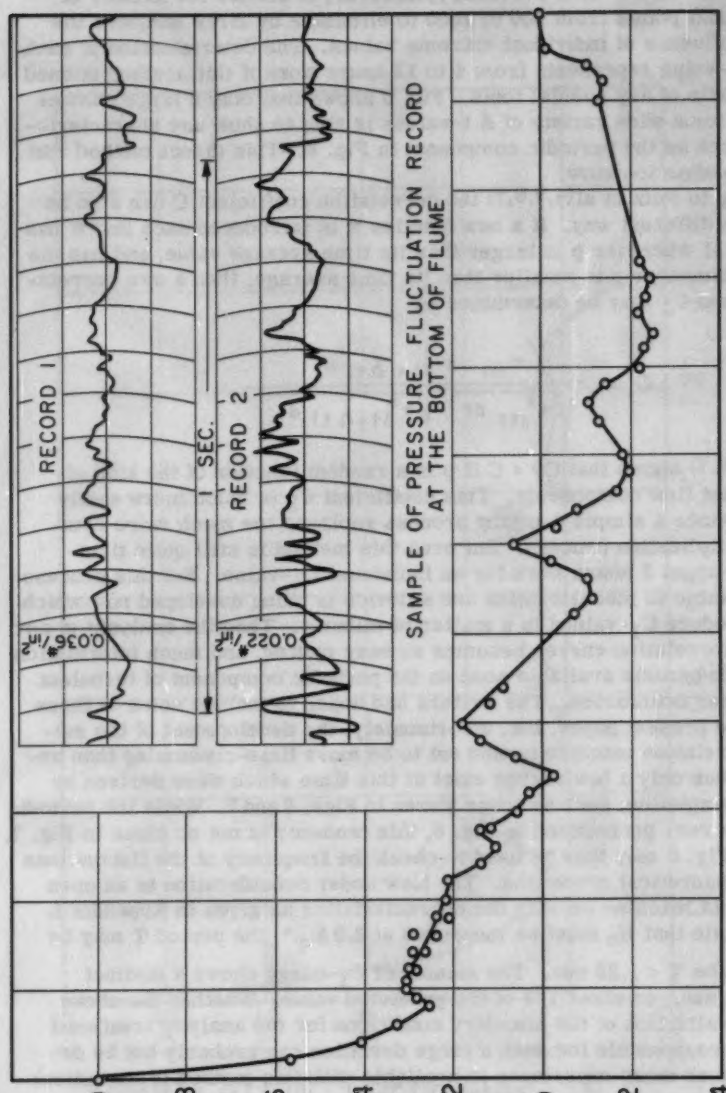

FIG. 6 AUTO-CORRELATION OF PRESSURE FLUCTUATION AT THE BOTTOM OF FLUME

and where the three integrals must cover the same range of t. It is obvious that the integral values may be approximated by the sum of a large number of individual p-values. It is necessary, however, to choose the number of these individual points from 200 to 1000 to eliminate by large numbers the accidental influence of individual extreme values. The determination of each individual C-value represents from 4 to 12 hours work if this method is used without the help of any special tools. Fig. 6 shows that only a large number of C-values for a wide variety of Δ t-values is able to show any characteristic trends such as the periodic component in Fig. 6. This direct method was thus abandoned as too slow.

According to Putz et al[4,5,6,7] the correlation coefficient C can also be obtained in a different way. If a new function π is introduced such that π has the value of +1 wherever p is larger than its time average value, and has the value of -1 wherever p is smaller than its time average; then a new correlation coefficient C_1 may be determined as

$$C_1 = \frac{\int \pi_{(t)} \; \pi_{(t+\Delta t)} \, dt}{\sqrt{\int \pi^2_{(t)} \, dt} \; \sqrt{\int \pi^2_{(t+\Delta t)} \, dt}}$$

Putz[4,5,6,7] shows that $C_1 = C$ if p is a random function of the kind of most turbulent flow components. This coefficient C_1 is much more easily determined since a simple counting process replaces the much more complicated multiplication process. But even this method is still quite time-consuming —about 2 hours work for an individual C_1-value. But this process is very adaptable to mechanization and a device is being developed now which is able to produce C_1-values in a matter of minutes. Then the analysis of any records by correlation curves becomes an easy matter, and much information is expected to become available soon on the periodic component of turbulent processes near boundaries. The writers had hoped to include some of these results in the present paper, but, unfortunately, the development of the mechanical correlation machine turned out to be more time-consuming than anticipated. Thus only a few curves exist at this time which were derived by manual determination, such as those shown in Figs. 6 and 7. While the periodic component is very pronounced in Fig. 6, this tendency is not so clear in Fig. 7. The flow of Fig. 6 may thus be used to check the frequency of the fluctuations against the theoretical prediction. The flow under consideration is an open channel flow of machine oil with the characteristics as given in Appendix I. Assuming again that U_o must be measured at $3.0\,\delta_T{}^*$, the period T may be calculated to be T = 1.25 sec. The measured C_1-curve shows a distinct period of 0.4 sec., or about 1/3 of the predicted value. Whether the above discussed idealization of the boundary conditions for the analytic treatment can be made responsible for such a large deviation can probably not be decided until much more experience is available with this method of statistical analysis.

K. Boundary Sublayer and Turbulence

In order to point out some of the relationships between the sublayer flow and the turbulence outside the sublayer, let us begin with the description of some of the characteristics of turbulence. Many definitions have been given

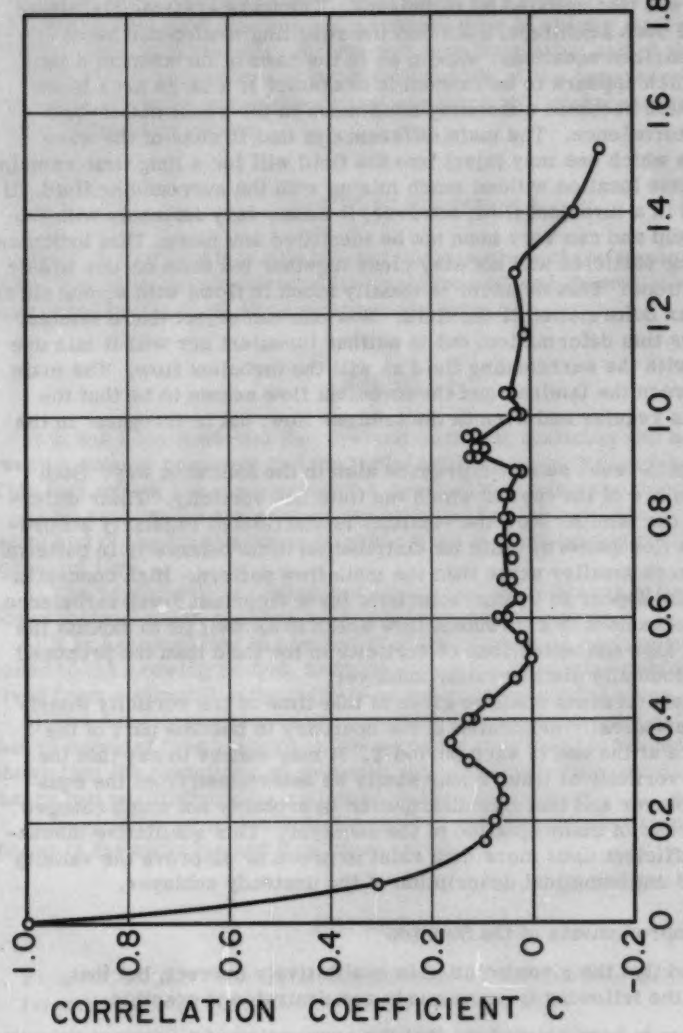

FIG. 7 AUTO-CORRELATION OF PRESSURE FLUCTUATION AT THE BOTTOM OF FLUME

of turbulence in the past, most of which stress the random character of the flow pattern in turbulence. Its detailed description still is made by means of the Navier-Stokes equations, however.

One of the most important characteristics of turbulence can be pointed out if a comparison is made between fluid agitated by simultaneous complicated wave systems and that agitated by turbulence. The wave systems visualized here may be of such amplitude, such that the resulting motion can be described by linearized equations. Again, as in the case of turbulence, a motion results which appears to be random in character if a large area is observed, and which becomes absolutely continuous in the small detail—and still, it is not turbulence. The main difference is that in case of the wave motion any dye which one may inject into the fluid will for a long time remain at about the same location without much mixing with the surrounding fluid. If dye is injected in a turbulent flow, however, it mixes very intensely with the surrounding fluid and can very soon not be identified any more. This indicates that neighboring particles will not stay close together but soon occupy widely separated positions. This behavior is usually found in flows with strong shear motion or shear deformation of the fluid. Now one can object that a laminar flow also shows this deformation, but is neither turbulent nor will it mix dye as efficiently with the surrounding fluid as will the turbulent flow. The main difference between the laminar and the turbulent flow seems to be that the shear motion is regular and even in the laminar flow, but is irregular in the turbulent flow.

This same difference can be expressed also in the following way: Both types of motion are of the type in which the fluid has vorticity. Their difference is that in the laminar flow the vorticity is distributed regularly according to the main flow pattern, while its distribution in turbulence is in patterns which are of much smaller scale than the main flow pattern. High concentrations of vorticity appear to be characteristic for a vigorous, fresh turbulence. There is no mechanism in a turbulent flow which is as well fit to explain the origin of these high concentrations of vorticity in the fluid than the proposed model of a periodically disintegrating sublayer.

No explicit expressions shall be given at this time of the vorticity distribution which periodically originates at the boundary to become part of the main turbulence at the end of each period T. It may suffice to say that the distribution of vorticity at time T may easily be determined from the equations of the sublayer and that this distribution is probably not much changed during the process of disintegration of the sublayer. This qualitative discussion may be sufficient until more data exist to prove or disprove the validity of the proposed mathematical description of the unsteady sublayer.

L. Possible Improvements of the Solution

It is believed that the given solution is qualitatively correct, but that, among others, the following improvements are desirable if possible:

1) It has already been pointed out that the assumption of a constant velocity in the turbulent flow adjacent to the sublayer is very artificial and has been introduced only for mathematical reasons.

2) It was assumed that the entire sublayer becomes part of the turbulent flow. It is possible that only the outer part of the sublayer becomes turbulent and that an inner part of the sublayer remains always at the boundary. Even if this steady part of the sublayer is very thin, it would materially change the constants calculated for δ_T^*, T, etc.

3) It is easily possible that the one-dimensional description of the sublayer growth is insufficient to predict the actual conditions if the real growth occurs not simultaneously over large areas of the boundary. It is conceivable that the process actually changes phase over the various parts of the boundary like a wave motion. Different solutions would result in that case.

4) It is most desirable that a description be found for the disintegration process as that part may occupy sufficient time to change materially the time average values of average velocity, velocity fluctuation and of the period T.

An intense qualitative and quantitative study of the processes as well as an extension of the proposed theoretical approach will be necessary to find answers to these questions.

ACKNOWLEDGMENT

Work on this problem was started under a grant of the Research Corporation. The later development of the experimental and theoretical work was sponsored by the U. S. Department of the Navy.

SUMMARY

1) It has been observed that dye and sediment particles are exchanged between a smooth boundary and the turbulent flow through the viscous sublayer. This fact makes the assumption of a quasi-steady sublayer impossible.

2) No reasonable explanation can be given for the creation of new turbulence and of the transmission of shear from a quasi-steady sublayer to the turbulent flow.

3) The periodically growing and disintegrating sublayer pattern is proposed instead which explains all these facts satisfactorily.

4) It is assumed that the period of disintegration is negligibly short compared to the growing period; average values for the entire period are thus derived from a simplified description of the growing period alone.

5) The most objectionable assumption made for mathematical reasons is that of constant flow velocity in the turbulent flow outside the sublayer. It is shown that the deviations of observed patterns from the prediction of the theory can qualitatively be explained by this assumption.

6) No qualitative contradiction has been found to date between the proposed theory of the sublayer and flow observations.

REFERENCES

1. Einstein, H. A.: "Der hydraulische oder Profil-Radius," Schweizerische Bauzeitung, Vol. 103, No. 8, February 24, 1934.

2. Peirce, B. O.: "A Short Table of Integrals," Ginn and Company, 1929.

3. Laufer, J.: "The Structure of Turbulence in Fully Developed Pipe Flow," NACA TN2945, June 1953.

4. Putz, R. R.: "Measurement and Analysis of Ocean Waves," Proceedings of the First Conference on Ships and Waves, Chap. 5 (Published by Council of Wave Research and Society of Naval Architects and Marine Engineers.) 1954.

5. Putz, R. R.: "Wave Transformation: Linear Least-Squares Predictions," Tech. Report Series 29, Issue 58, Institute of Engineering Research, University of California, Berkeley - pg. 4, 1954.

6. Putz, R. R.: "Statistical Analysis of Wave Records," Proceedings of the Fourth Conference on Coastal Engineering, Chap. 2, Council on Wave Research, 1954.

7. Lawson, J. L. and Uhlenbeck, G. E.: "Threshold Signals," McGraw Hill, N. Y., 1950.

8. Li, H.: "On the Measurement of Pressure Fluctuations at a Smooth Boundary of an Incompressible Turbulent Flow," Contract N-onr-222(22), Project Nil 062 173, Report Series No. 65, Issue No. 1, Institute of Engineering Research, University of California, Berkeley, December 1954.

APPENDIX I

Experimental Procedure used in the Determination of Local Wall Pressures

After the problem as such was conceived about three years ago a search was made of various pressure recording devices, i.e., devices which can be used to record continuously the instantaneous pressure and its fluctuations as they apply to a small part of the boundary surface of a turbulent flow. An appraisal was made of the frequencies which must be expected to occur in the problem, of the magnitude of the amplitudes of the fluctuations and of the area which might be expected to show predominately equal pressure. On the basis of water flowing at Reynolds numbers of about 10^4 to 10^5 the following specifications were drafted for the pressure gage:

Frequency response	0 to 5000 cps
Pressure sensitivity	±0.001 psi
Maximum pressure	1 psi

Area covered by the sensitive element 0.001 Ft. Diameter

No instrument could be found commercially which satisfied these stringent conditions even approximately. It was thus decided to acquire the one which approximated the conditions the closest. It was hoped that either the estimated conditions were too stringent or that the instrument could be improved later to adapt it to the particular purpose.

The best prospect was at the time a Rutishauser transducer. This instrument uses a membrane of 0.0156 ft. free diameter which has a frequency response up to 10,600 cps and a normal sensitivity of 0.01 psi with a maximum pressure of 1 psi using a diaphragm of 0.001 inches thickness. It may easily be seen that this instrument is still far from satisfying the original conditions, but it appeared to have the best performance characteristics of any instruments then on the market. The membrane together with an electrode 0.0016 inches behind it represent a variable condenser which is used to modulate the

frequency of a 10 megacycle oscillator. The output of this oscillator is then analyzed by a discriminator resulting in a D-C output signal proportional to the original motion of the diaphragm. This electric signal was then amplified and recorded or its RMS value measured. For the details of the electronic system the reader is referred to report (LI, 1954).[8]

With this kind of instrument it is possible to adjust the useful ranges somewhat. If the sensitivity is to be increased, for instance, this can be done by replacement of the diaphragm by another one of smaller thickness. Unfortunately, this change also reduces the frequency response, such that sensitivity can be gained by increased amplification until the unavoidable tube noises become excessive. The area of measurement can be reduced by mounting the diaphragm inside a cavity, which itself is connected with the free flow by a small opening. Again, the reduction of measuring area is traded for frequency response, which is drastically reduced by the cavity. For the theory of the cavity, the reader is again referred to report by LI.[8]

A very important and extremely time consuming phase of the experimental work was the calibration of the pressure indicator and its complex electronic amplifying and recording system. This calibration could not be made with one piece of equipment for the entire range, but was divided into a number of independent stages:

1) A static calibration was made by direct comparison with manometer readings under use of DC-amplifiers. Only limited sensitivity can be reached by this method because of the difficulty of stabilizing high gain DC amplifiers.

2) A low frequency calibration was made by means of a mechanically driven excenter which periodically compressed the air enclosed in a bellows. Frequencies up to 160 cps could be reached with this instrument which automatically governed the amplitude independent of the frequency.

3) A high-frequency vibrator was used for frequencies between 130 and 6000 cps. This system consists of a loud speaker driving various resonance tubes, in the bottom of which the pressure heads were mounted.

The calibration procedure became complicated not only due to the use of the different instruments but also because the third method does not permit an absolute calibration but only a relative comparison of various instruments.

The calibration of the transducers with the membranes directly exposed to air was performed first. The first two methods which permit an absolute calibration showed that both pressure heads with all available diaphragms gave a perfectly straight response up to the maximum frequency of 160 cps. The theoretical limit of linearity can be predicted to be 3500 cps for the thinnest membrane. It would be expected that if any deviation from the straight calibration would occur in the range of frequencies between 160 cps and the frequencies where resonance begins to affect the calibration, such deviation would change with the instrument and particularly with the thickness of the membrane. It could be expected that the calibration was still straight for both instruments as long as their signal was the same for a given signal in the resonance tube. By means of this method the instruments were shown to have a straight frequency response up to a frequency of 2000 cps for all diaphragms in air.

Diaphragm No.	Range psi	Thickness in.	Dia of Diaphragm in.	Natural Freq. in Air cps	Linearity Limit in Air cps	Dia. of Meas. hole in.	Length of Cavity in.	Predicted Natural Freq. in Water cps	Linearity Limit in Water cps
1	0-1	0.001	3/16	10,600	3,500	0.1	1/32	3570	1190
							1/16	2590	860
							1/4	1320	440
							1	660	220
						0.01	1/32	380	126
							1/16	260	88
							1/4	132	44
							1	66	22
1	0-100	0.004	3/16	42,600	14,200	0.1	1/32	24,800	8,260
							1/16	19,100	6,360
							1/4	10,400	3,470
							1	5,320	1,770
						0.01	1/32	3,050	1,020
							1/16	2,140	714
							1/4	1,020	360
							1	540	180

The next step in the calibration was the introduction of a cavity filled with liquid with a reduced opening to the open fluid in which the pressures are measured, reducing the area over which the pressure is averaged. The additional drastic reduction of the frequency response which the theory of the cavity predicts was actually found to occur by this measurement. The table on the preceding page gives the frequency response for various geometries of the cavity.

The Experiments

The previously enumerated values for the qualifications of the measuring device are compared with the values as found to characterize the instruments by their calibration one finds that

1) For a given opening of the measuring cavity the frequency response is reduced considerably for a significant part of the active spectrum.
2) The sensitivity of the device is barely sufficient to separate the expected signal from unavoidable noise.

This state of affairs appeared to prove the chosen instrument to be utterly unsatisfactory. Before the entire approach was changed it was decided to try if possibly at least certain partial problems or certain ranges of conditions could be investigated by the available instrumentation. Thus, the question was asked under which conditions large scale of the turbulence pattern near the wall is combined with low frequencies and high pressure scales. The only possible answer is a flow with low Reynolds number and high viscosity—a flow of a highly viscous fluid. After previous attempts had already shown that closed pipe systems are very difficult to be freed from all kinds of pressure waves which constantly travel through the system and would distort the pressure records, it was decided to construct an open channel flume circulating a flow of oil at high velocity, but moderate Reynolds number.

The flume with a rectangular cross section of 11.5 inches clear width and 8 inches depth was constructed of wood, supported by timber bents. The oil dropped from the flume into a reservoir from which it was pumped by an electrically driven centrifical pump through a 10 inch pipe to the upstream end of the flume. The discharge was adjusted by by-passing part of the discharge directly into the reservoir. One of the most important features of the system was the complete mechanical separation of the flume proper from the pump and the return pipe to keep all vibrations away from the flume and the pressure recording instrument which is very sensitive to vibrations of any kind. The discharge was measured at a contraction of the return pipe; the oil depth in the flume by point gages. A continuous record was kept of the oil temperature, from which the viscosity could be determined after a set of viscosimeter tests had determined the viscosity-temperature relationship for the particular oil. For engineers who are accustomed to work with water flows, the resulting flow was rather odd: with respect to turbulence the flows were near critical, i.e., from laminar through critical to turbulent, had about 2 inches depth of flow and velocities of 6 to 7 ft/sec., and was thus flowing with velocities significantly higher than wave velocity, or with other words a laminar shooting flow was very readily obtained.

This experimental arrangement had another great advantage. A laminar flow was first established with velocities close to critical and the pressure recording instruments turned on such that the noise level could be observed

as it was generated by the pump and pipeflow and by other unrelated activities in the neighborhood. Then, the flow was slightly increased to cause turbulence to be generated and the record continued while the flow measurements were made. It could be observed that the pressure records showed fluctuations due to turbulence of a larger order of magnitude than the general noise level.

Experimental Conditions for the Flow of Fig. 6.

The following flow conditions were established

Channel width	b	$= 0.957$ ft.
Channel slope	S_o	$= 0.0502$
Flow depth	h	$= 0.144$ ft.
Flow velocity	U_{av}	$= 6.27$ ft/sec
Discharge	α	$= 0.865$ cfs
Viscosity of oil	μ	$= 1.23 \times 10^{-3}$ lb. sec/ft^{-2}
Density of fluid	ρ	$= 1.73$ slugs/ft^3
Kinematic viscosity	ν	$= 7.15 \times 10^{-4}$ ft^2/sec

If the shear is assumed to be evenly distributed over bottom and sides, the average shear stress $\overline{\tau}_o$ is

$$\overline{\tau}_o = 0.313 \text{ lb/ft}^2$$

$$\overline{\tau}_o/\rho = 0.180 \text{ ft}^2/\text{sec}^2$$

Shear velocity $u_* = \sqrt{\overline{\tau}_o/\rho} = 0.423$ ft/s.

Thickness of the viscous sub-layer as conventionally defined is

$$\delta = 11.6\, \nu/u_* = 1.96 \times 10^{-2} \text{ ft.}$$

The period of sub-layer growth and separation frequency are for various U_o

U_o at $0.5\, \delta_T{}^*$	$T = 0.524$ sec	$n = 1.91$ sec^{-1}
U_o at $1.0\, \delta_T{}^*$	$T = 0.780$ sec	$n = 1.28$ sec^{-1}
U_o at $2.0\, \delta_T{}^*$	$T = 1.07$ sec	$n = 0.935$ sec^{-1}
U_o at $3.0\, \delta_T{}^*$	$T = 1.25$ sec	$n = 0.800$ sec^{-1}

Since the flow could not be maintained for a very long time for various practical reasons it was decided to record continuously the pressure for several minutes and to postpone the analysis of the record for a later time.

The block diagram of the experimental equipment is shown in Fig. 8.

The Tektronix low level preamplifier type 122, which amplifies the discriminator voltage, has a noise level as low as 1 to 4 microvolts expressed as input signal. The preamplifier has a maximum gain of approximately 1000, the frequency response curve is essentially flat from 1 cycle per second to 40 kilocycles per second.

The output signal of the preamplifier was further amplified in a brush

universal analyzer and recorded by a Brush magnetic oscillograph BL-202. The Brush universal analyzer is a D-C amplifier and has a frequency response which is flat from zero to 100 cps. For higher frequency signals a DuMont Cathode-Ray Oscillograph type 304-A was used to replace the Brush universal analyzer, in connection with a DuMont oscillograph recording camera type 321. A short excerpt of this record is given in Fig. 5.

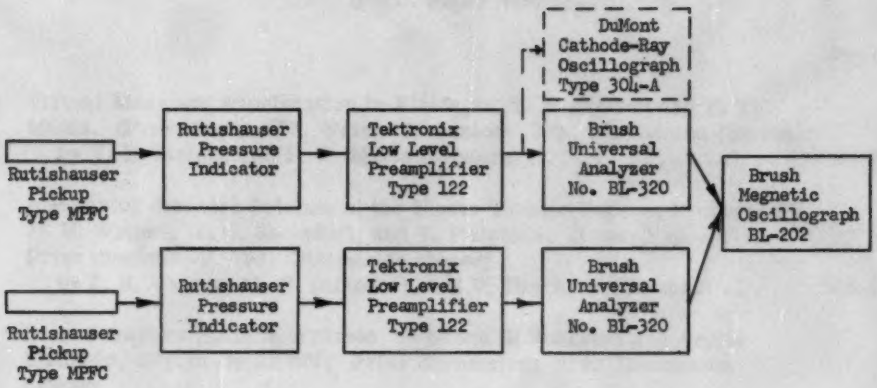

FIG. 8

Block Diagram of Equipment for
Pressure Fluctuation Measurement of two points.

JOURNAL
ENGINEERING MECHANICS DIVISION
Proceedings of the American Society of Civil Engineers

CONTENTS

DISCUSSION
(Proc. Paper 946)

JOURNAL

ENGINEERING MECHANICS DIVISION

Proceedings of the American Society of Civil Engineers

CONTENTS

DISCUSSION
(Proc. Paper 940)

Note: Paper 940 is part of the copyrighted Journal of the Engineering Mechanics Division of the American Society of Civil Engineers, Vol. 82, EM 4, October, 1956.

Discussion of "VIRTUAL MASS AND ACCELERATION IN FLUIDS"

by T. E. Stelson and F. T. Mavis
(Proc. Paper 670)

T. E. STELSON,[1] J.M. ASCE, and F. T. MAVIS,[2] M. ASCE.—The writers' data on added mass of rectangular parallepipeds with square side moving broadside-on (Fig. 4) have added meaning as they have been replotted by Mr. Caldwell. Using the ratio of added mass to displaced-volume mass as ordinate he shows quantitatively in his Fig. 5 what every canoeist has experienced—namely that for the same acceleration it takes much more force to push a paddle through water broadside-on (small relative length) than feathered (large relative length). Figs 4 and 5 show the same experimental data for rectangular parallepipeds—but Mr. Caldwell's Fig. 5 shows them more clearly. The data can be formulated as follows:

$$\frac{c}{\rho V} = 0.67 \left(\frac{d}{w}\right)^{-0.94}$$

where

c = added mass
ρ = mass density of the fluid
V = volume of fluid displaced
d = thickness in the direction of motion
w = broadside width of square face.

Mr. Silberman questions these statements in the introduction to the paper:

> "Determination of added mass by experiment often has been inconsistent and unreasonable. Measured values for added mass have usually been larger than can be explained by theory and analysis."

Each sentence is merely a statement of fact as the writers intend it—and the second is not a conclusion drawn from the first as Mr. Silberman may have inferred. In fact the data shown in Mr. Silberman's Fig. 6 eloquently supports both statements.

First, what was measured and plotted in Fig. 6 is expressed as a drag coefficient—a variable which mixes velocity-dependent and acceleration-dependent forces inseparably. What the writers measured and reported in Figs. 2, 3 and 4 of the paper was an "added-force" term that was only acceleration-dependent, because in their experiments accelerations were

1. Asst. Prof. of Civ. Eng., Carnegie Inst. of Technology, Pittsburgh, Pa.
2. Prof. and Head, Dept. of Civ. Eng., Carnegie Inst. of Technology, Pittsburgh, Pa.

high and velocities were low. In fact the writers consider this separation and control of variables—variables that have commonly been masked in earlier experiments—to be one of their more important contributions to experimental studies of virtual mass.

Second, every point except one as plotted in Mr. Silberman's Fig. 6 shows the "drag coefficient" to be substantially higher than the solid line (1) designated "C_D (attributable to added mass). . . ."

Thus, Mr. Silberman's Fig. 6 says in the language of graphs the same thing as the writers' two sentences say in the language of words—both essential "languages" of the engineer.

There seems to be abundant other evidence in the literature since 1779 to support the statement that "determination of added mass by experiment often has been inconsistent and unreasonable." Yet many early investigators of virtual mass deserve great credit for their keen observation and analysis of fundamentals that are so elusively hidden by the simultaneous influence of uncontrolled variables. One of these was F. W. Bessel* who, in 1828, reported that because of added mass the period of pendulums was increased from one part in 3,000 to one part in 35,000. It is a tribute to Bessel and his experimental technique that he was able to detect such slight changes; and yet it is not surprising that from such relatively small quantitative measurements he should have arrived at deduced added masses that were as much as 90 per cent larger than can consistently and reasonably be expected nowadays.

Incidentally, all but two points shown in Mr. Silberman's Fig. 6 are from 100 per cent to 1000 per cent higher than the dotted curve marked "(1) + (2)" which, presumably by his hypothesis, should represent the drag coefficient for steel spheres accelerated indirectionally.

The closing suggestion by Mr. Caldwell, namely, to study ". . . the problem of a fixed object held in an accelerating flow,"—particularly in a closed conduit—may resolve whatever differences of interpretation there may be between Mr. Silberman and the writers. It is because of differences in analytical and experimental studies that engineers can acquire a better understanding of accelerated motion of structures and machines in fluids—and of the associated forces they must anticipate in design.

* Bessel, F. W., "Untersuchungen über die Länge des einfachen Secundenpendels." Abhandl.d. Akad. d. Wissensch. (Berlin) 1-256 (1828). Described in English by F. Baily in Trans. Roy. Soc. London, 399-492 (1832).

Discussion of "A RESISTOR-NETWORK SOLUTION OF THE ELASTO-PLASTIC TORSION PROBLEM"

by J. H. Weiner, M. G. Salvadori, and V. Paschkis
(Proc. Paper 671)

J. H. WEINER,[1] M. G. SALVADORI,[2] M. ASCE, and V. PASCHKIS.[3]—The writers wish to thank Mr. Moos for his interesting comments and questions concerning the paper. His first suggestion for obtaining a more accurate value of the roof slope by extrapolation is certainly feasible theoretically. If the solutions corresponding to the two mesh sizes were obtained numerically, the procedure would be completely practical since it is then known that the entire error in each solution (except for the minor round-off error) is due to the finite mesh size. However, if the solutions are obtained by a network, there is, in addition, a small experimental error which is not a function of mesh size, and this error may cause large errors in any extrapolation procedure.

His question regarding the extension of the use of resistor networks into other areas is one which has occupied the interest of the Heat and Mass Flow Analyzer Laboratory for some time. Development is now under way on their use in the solution of thermal stress problems and in the determination of stresses in thin shells. The writers hope to be able to report on these activities in the future.

In regard to his third question, work has continued since the presentation of the paper on the direct determination of $\Sigma\ e_i$ (Eq. 5 '''), and two successful techniques have been developed. The measurement of $I_0 - I$ directly was first tried by a circuit, Fig. a, which seems simple and attractive. The resistance R_0 equals the equivalent resistance of the network from the voltage source, E, to ground if all the nodes of the circuit are grounded. The resistance R_A is the equivalent resistance of the network with e_i at their proper values. If $r_a = r_b$ and if $R_A = R_0$, the reading of Δ is 0. Thus by using a variable resistor in place of R_0, its proper value can be set by having R_A with $e_i = 0$ and adjusting R_0 until $\Delta = 0$. The current in R_A equals that in R_0 and is I_0. Then, without changing the setting of R_0, the values e_i and R_A are allowed to take their proper values and Δ is read. The current in R_A is now I. One finds

$$\Delta = r_b (I_0 - I) \qquad (1)$$

1. Asst. Prof. of Civ. Eng., Asst. Technical Director, Heat and Mass Flow Analyzer Lab., Columbia Univ., New York, N. Y.
2. Prof. of Civ. Eng., Columbia Univ., New York, N. Y.
3. Adjunt Associate Prof. of Mechanical Eng., Technical Director, Heat and Mass Flow Analyzer Lab., Columbia Univ., New York, N. Y.

if I_o is the current in R_o and I the current in R_A.

However, a mathematical analysis shows that even very small errors, resulting for example from $r_a + r_b$ or from $\Delta + 0$ when adjusting R_o, cause errors in Δ of the order of magnitude of 20 - 30%.

Therefore two methods were developed, both of which yield the required sum of the nodal values of e_i directly. One method consists of an integrating device, attached to the voltmeter. In the present case a Leeds and Northrup Speedomax recorder, type G, was used through the isolating amplifiers normally employed in the Heat and Mass Flow Analyzer. The integrating device is mounted on the instrument, which is successively connected to each node and permits direct reading of the total voltage, without reading and recording the individual values. The integrator actually integrates voltage-time. Therefore the meter is kept on each point for a constant length of time, and the integral is then divided by this constant time. Although very brief times would theoretically be sufficient, it has been found that more reliable results are obtained if the constant time on each point is 40 seconds or more.

The integrator result compared with the sum of voltages obtained by reading and adding all voltages arithmetically is accurate to within $\pm$ 1.7%.

Another method of obtaining voltages directly consists in connecting a very high resistance, R_M, to each node. All these resistances are then connected together and grounded through an additional resistor, R_C, which is calibrated accurately (Fig. b). The voltage drop through R_C is proportional to the sum of the currents from the several nodes, and each current is proportional to the voltage of this node, provided that the voltage at the junction of R_C and R_M is negligible in comparison with the nodal voltages e_i. Values of R_M must be chosen high enough to prevent an influence on the value of e_i. It has been found that if R_M is 1000 times higher than the resistance R (Fig. 3, original paper) results are satisfactory; in the present case R_M was 10,000 times higher than R_C. The sum of the voltages thus determined was within 0.5% of the sum of the individual voltage readings determined arithmetically.

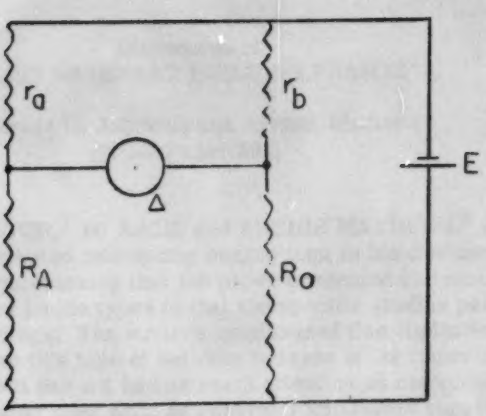

Fig a

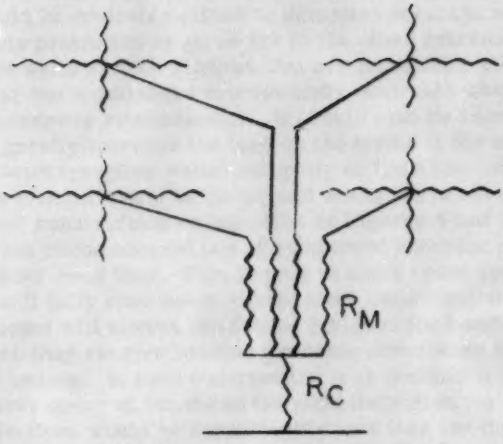

Fig. b

Discussion of
"BLAST RESISTANT BUILDING FRAMES"

by Bruce G. Johnston and Archie Mathews
(Proc. Paper 695)

BRUCE G. JOHNSTON,[1] M. ASCE, and ARCHIE MATHEWS,[2] J.M. ASCE.— Mr. McKee has contributed interesting suggestions in his discussion and is entirely correct in emphasizing that the paper presented an incomplete picture of blast resistant frame types in that the specific studies pertain to a limited class of buildings. The writers emphasized this limitation themselves at the outset but chose this type of building because of its importance to heavy industry and because it has not had as much attention as completely protective construction. The paper does provide generally applicable suggestions regarding design for maximum structural strength and deformation leading to improved plastic behavior of steel beams, steel columns, beam columns, compression details, and connections; that are applicable to other types of blast resistant steel construction in addition to the completely frangible wall type of building that was used as a design example.

Although, as Mr. McKee points out, the majority of structures have walls with windows and may therefore be assumed to be partially open, the writers believe that in buildings that are specifically designed for strong blast exposure it would be desirable either to minimize openings and design the walls for complete protection or go as far to the other extreme as is practicable and provide walls and/or windows that are frangible. Mr. McKee advocates use of shear walls and these are certainly desirable where not prohibited by interior accessway requirements. It should also be recognized that shear walls will greatly increase the load on the frame if the blast wave strikes the structure (with frangible walls) obliquely or from the end. From this point of view cross bracing would be better and would serve essentially the same purpose in steel construction as indicated in Figures 4 and 5. Mr. McKee suggests that the recommended use of reinforced concrete roof slabs may lead to collapse under dead load. This is true in some cases for non-continuous framing but if fully continuous welded steel construction is adopted, the exterior columns will always need to be designed for bending as well as direct stress since they receive bending moments distributed to them from the ends of the roof beams. In such construction it is doubtful if collapse due to dead load will ever occur at ten times the yield deflection for the outside columns. These deflections would be considerably less than ten times the yield deflection for the interior columns, which might be 8WF31 sections as suggested by Mr. McKee.

Mr. McKee suggests the use of members of circular cross section because the drag coefficient would be only 0.35. The hollow circular section is an

1. Prof. of Structural Eng., Univ. of Michigan, Ann Arbor, Mich.
2. Research Aide, Dept. of Theoretical and Applied Mechanics, Univ. of Illinois, Urbana, Ill.

excellent structural member but there are several reasons why it is not used to a greater extent. There is difficulty in the design and fabrication of connections. If welding is used this difficulty may very largely be overcome. The greatest deterrent to use of circular members, however, is the fact that their cost per pound greatly exceeds that of the open rolled structural shape. It is also incorrect to state that the drag coefficient of circular members is 0.35 without some qualification. The drag coefficient is dependent on the Reynolds Number and this is especially true in the case of circular cylindrical shapes. For example, a 2 1/2" diameter round cylinder with a wind velocity of 100 miles per hour will have a drag coefficient of 1.20 and it is only for a considerable increase in size that the drag coefficient theoretically reduces to 0.35. In practical applications this may be on the low side because of the effect of surface roughness in increasing the drag coefficient as compared to coefficients obtained on machine made wind tunnel models.

Proposed equivalent static lateral loads for frames supporting frangible wall construction were advanced as tentative only. Mr. McKee agrees that design for such loads will improve the blast resistance. In an actual war emergency the uncertainty as to size, location, and other factors associated with possible bomb detonations affecting a building in or very near a target area makes the value of precise dynamic analyses questionable. There has been no great evidence of desire on the part of builders of industrial plants to do very much in the way of strengthening structures against nuclear blast. In view of this situation it seems to the writers that best that can be generally hoped for at the present time is to introduce those improvements in blast resistance that can be obtained at a reasonable cost and that will effectively reduce the probable area of total destruction. It may be that variations in bomb parameters will alter the relative chance for structural survival of a specific structure but the over-all result will be to reduce damage in critical areas. If the builder can follow the government recommendation to disperse his plants to a region at some distance from critical areas it would of course be desirable to consider gradually reduced levels of protective requirements. Recommendations for such reduced levels of design load will probably become available through future government publications.

The writers do not belittle in any way the importance of dynamic analyses especially as a background for research and for the setting up of standards for bomb resistant construction. In the end, however, regardless of what approach is used, the engineer will usually select column and beam sizes by use of some sort of equivalent static design load. If he uses charts that are available as mentioned by Mr. McKee for the solution of simple problems he is in effect using the results of prior dynamic analyses to establish the equivalent static loads that he will now use to proportion the structure.

Mr. McKee obviously has a background of study and research in the field of blast loaded structures. In general his remarks have been constructive and his suggestions as to limitations inherent in some of the ideas expressed by the writers are well taken and should receive consideration.

Discussion of
"FLOW INTO A WELL BY ELECTRIC AND MEMBRANE ANALOGY"

by Chong-Hung Zee, Dean F. Peterson, and Robert O. Bock
(Proc. Paper 817)

ROBERT E. GLOVER,[1] M. ASCE.—The ingenious electric analog arrangement described by the authors facilitates the investigation of flow conditions near a well in an aquifer which has no upper confining bed. Such devices often fill a need since the formulas commonly used for engineering purposes are based upon simplifications and approximations which exhibit their greatest short-comings in this area.

A common idealization is based upon the following simplifying assumptions:

a) The gradient of the free surface is conserved throughout the depth of the aquifer.
b) The reduction of the area available for the flow of ground water due to the depression of the free surface, as the well is approached, is neglected.

These two assumptions are equivalent to the single requirement that the draw-down everywhere should be small compared to the original depth of water in the aquifer. The draw-downs in actual wells often exceed these limitations and provide an inducement to seek for more elaborate solutions which will provide closer approximations. However, many actual cases involve transient phenomena and the added mathematical difficulties introduced by the time factor provide powerful inducements for retaining the simple idealization just described. The best way out of these difficulties seems to be to use this simple idealization as long as the draw-downs retain tolerable values and to supplement these solutions with a special investigation in the zone of large draw-down near the well. The electric analog device described should provide a means of making this special investigation and there is good reason for believing that, under certain identifiable conditions, this treatment will be adequate even though transient conditions must be dealt with.

If y represents the draw-down, or lowering, of the free water surface in an aquifer having an initial water depth D, a permeability K and a ratio of drainable voids to total volume v the simple idealization described yields the following expression for the condition of continuity:

$$\frac{\partial y_1}{\partial t} = \frac{KD}{v}\left(\frac{\partial^2 y_1}{\partial r^2} + \frac{1}{r}\frac{\partial y_1}{\partial r}\right). \qquad (a)$$

For a steady state the right hand member is zero and a comparison with the Author's equation (5) will show that, if the weight of the membrane is neglected, the differential equations are of the same form. It follows that the

1. Research Eng., Bureau of Reclamation, U. S. Dept. of the Interior, Denver, Colo.

membrane can take forms which represent very closely the draw downs obtained from this idealization. The steady state solution of equation (a) which corresponds to the Author's equation (1) is:

$$y_w - y = \frac{Q}{2\pi KD} \log_e\left(\frac{r}{r_w}\right). \qquad (b)$$

where y_w represents the draw down at the well.

The transient state solution for the case of a constant rate of withdrawal Q from a well of radius r_w is given by the well known exponential integral formula.[2]

$$y = \frac{Q}{4\pi KD} \int_{\left(\frac{vr^2}{4KDt}\right)}^{\infty} \frac{e^{-u}}{u} du . \qquad (c)$$

It has been noted by Taylor and Rainville[3] that if this integral is expressed in the usual series form, in terms of powers of the quantity which appears as the lower limit of this integral, plus a logarithm term and a constant, the terms of the power series tend to vanish as time increases because the time appears in the denominator. The last term to disappear is the one which is raised to the first power. If this term is retained and two values of y are subtracted an expression of the type of (b) above is obtained together with the difference of the two first power terms and it can be seen that the transient case reverts to steady state behavior, between the radii r_w and r_2, when

$$\frac{v(r_2^2 - r_w^2)}{4KDt} \text{ is small compared to } 2\log_e\left(\frac{r_2}{r_w}\right). \qquad (d)$$

It is inferred from these results of the approximate theory that if r_2 represents a radius at which the draw-downs remain small compared to D, a steady state continuous with the solution (c) at $r = r_2$ may be constructed in the interval r_w to r_2, by electric analogy or other means to properly represent the true conditions between r_w and r_2 at that time.

What constitutes satisfaction of the requirement (d) in any given case must be decided on the basis of the accuracy desired or attainable. It may be remarked that the aquifers found in nature often depart materially from the homogeneity postulated in the idealizations and through these irregularities often set a limit to the accuracy which may be attained.

2. THEIS, C. V. "The Relation between the Lowering of the Piezometric Surface and the Rate and Duration of Discharge of a Well using Ground Water Storage." Transactions of the American Geophysical Union 1935.
3. TAYLOR, W. H. and RAINVILLE, E. D. "Analysis of Pumping Test----" Informal memorandum., Bureau of Reclamation, Denver, Colorado, Feb. 2, 1937.

VAUGHN E. HANSEN,[1] J.M. ASCE.—It is indeed encouraging to note the progress which is being made to solve the complex problem of the hydraulics of unconfined wells. Very significant steps have been taken since the writer applied the membrane analogy to wells[2] and introduced the concepts of the discharge and well parameters.[3] The experimental data obtained recently by several investigators has added considerably to our knowledge of unconfined wells. The design curves of figures 9 and 12 are very useful and valuable summaries of this experimental data.

In reviewing the dimensionless plottings of the free-surface profiles shown in figure 9, the writer was of the opinion that plots of this nature would become even more useful and meaningful if parameters could be selected which reflected a better picture of the actual free-surface profile. The disadvantage of basing the profile upon an arbitrary radius of 115 times the well radius could also be avoided by such a procedure.

In further consideration of this need it appeared reasonable that the following functional relationship of well variables would uniquely define the free-surface profile:

$$f_1 (h, r, r_w, h_s, h_w) = 0 \qquad (1)$$

where all symbols are the same as originally defined by the authors. The variables of equation (1) can be grouped in dimensionless form as follows:

$$f_2\left(\frac{h}{r_w}, \frac{r}{r_w}, \frac{h_s}{r_w}, \frac{h_w}{r_w}\right) = 0 \qquad (2)$$

Since four quantities are still too many to clearly plot on a two-dimensional graph, the following combination of the four parameters of equation (2) was considered in an attempt to find three parameters which would give the desired picture of the free-surface and also provide a unique solution.

$$\frac{h-h_w}{r_w} = f_3\left(\frac{r}{r_w}, \frac{h_s-h_w}{r_w}\right) \qquad (3)$$

The grouping of parameters shown in equation (3) when plotted with $(h-h_w)/r_w$ as ordinate and r/r_w as abscissa with a family of $(h_s-h_w)/r_w$ curves would give the desired picture of the free-surface drawdown as the water approached the well. The question remained to ascertain if equation (3) would yield a unique solution.

To determine the uniqueness of equation (3), the values of the three dimensionless parameters were computed for three profiles contained in Mr. Zee's

1. Prof. of Irrig. and Drainage Eng., Utah State Agricultural College, Logan, Utah.
2. "Complicated Well Problems Solved by the Membrane Analogy," by Vaughn E. Hansen. Transactions, Am. Geophysical Union, Vol. 33, No. 6, Dec., 1952.
3. "Unconfined Ground Water Flow to Multiple Wells," by Vaughn E. Hansen, paper No. 2571, Vol. 118, Transactions, American Society of Civil Engineers, 1953.

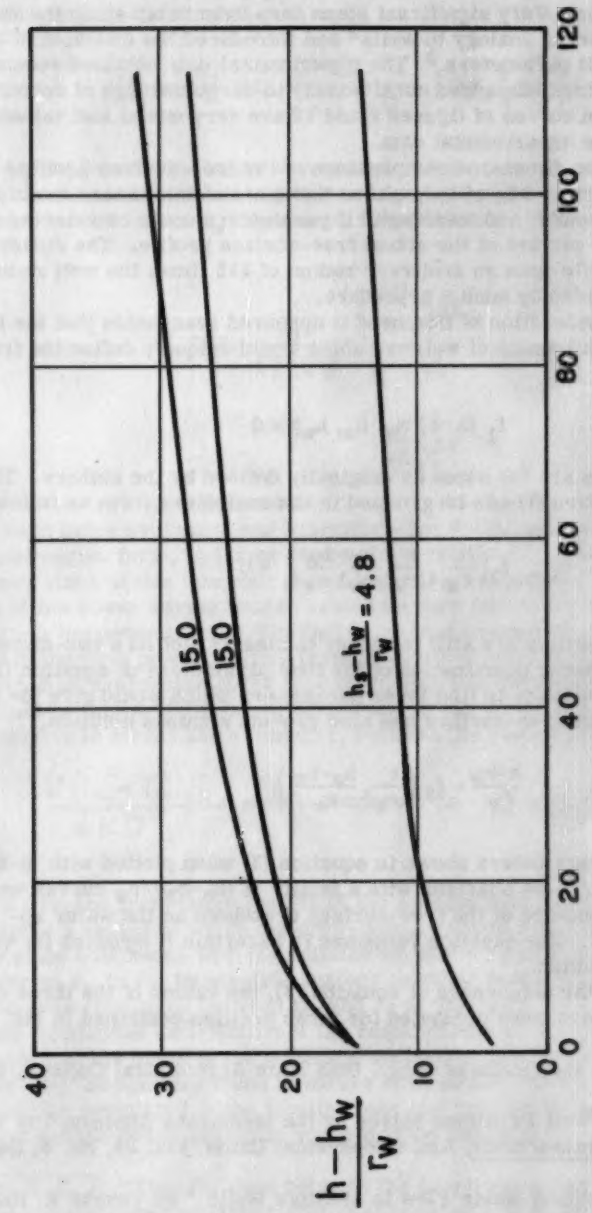

Fig. A. Dimensionless Plotting of Free-Surface Profile.

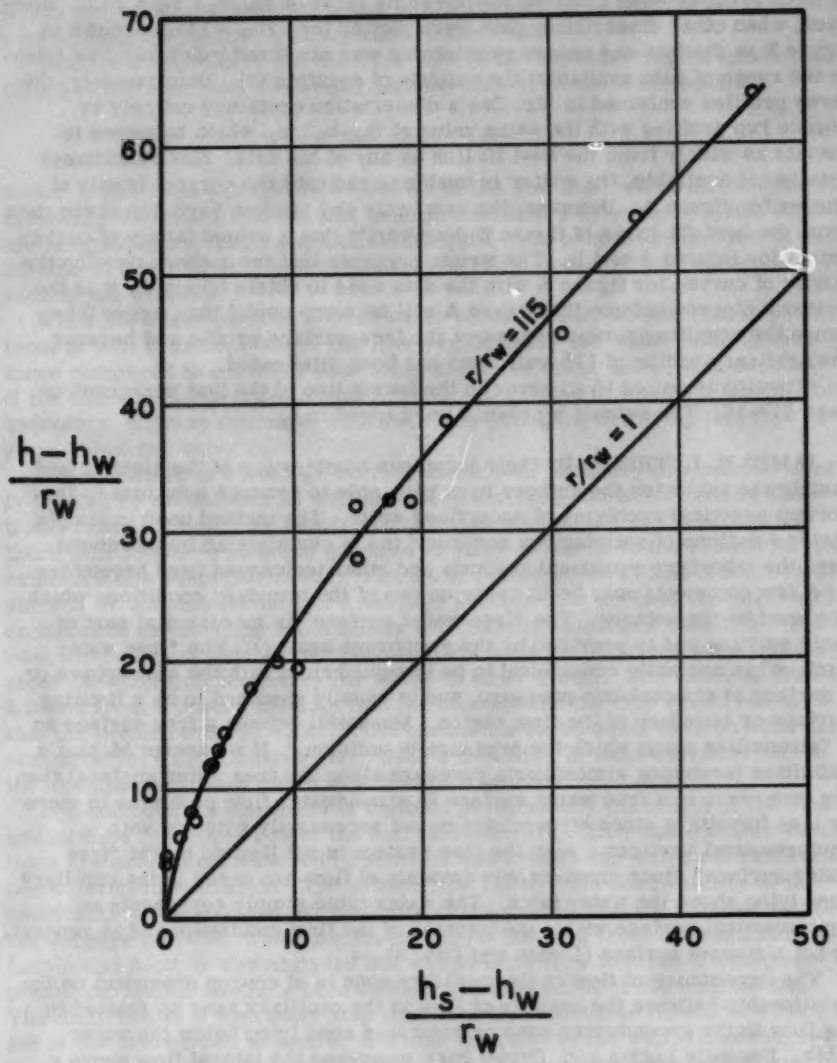

Fig. B. Well Parameters of Equation (3)

dissertation.[4] The results are shown in figure A. It is apparent that two free-surface profiles were obtained for the same value of $(h_s-h_w)/r_w = 15.0$. However, when other dissertation data were plotted for $r/r_w = 115$ as shown in figure B, a distinct and unique relationship was observed which varifies (within the range of data available) the validity of equation (3). Unfortunately, the three profiles contained in Mr. Zee's dissertation contained entirely by chance two profiles with the same value of $(h_s-h_w)/r_w$ which happened to deviate as widely from the best fit line as any of his data. Since additional data is not available, the writer is unable to indicate the correct family of curves for figure A. However, the proximily and random variation of the data from the best-fit curve of figure B does verify that a unique family of curves exists for figures A and B. The writer suggests that the authors develop the family of curves for figure A with the data used to obtain figure 9. It is the writer's sincere opinion that figure A will be more useful than figure 9 because the resulting curves represent the free-surface profile and because the arbitrary radius of 115 well radii has been eliminated.

Attention is called to an error in the fourth line of the last paragraph on page 817-10. The symbol h_w should be changed to h_s.

JAMES N. LUTHIN.[5]—By their ingenious combination of the electric and membrane analogies the authors have been able to produce solutions to important practical problems of unconfined wells. The method used is simple, yields solutions of satisfactory accuracy and is certainly an improvement over the laborious numerical methods and other techniques used heretofore.

A few comments may be in order on two of the boundary conditions which are used by the authors. The "free water surface" is an essential part of their solution and is provided by the membrane analogy. The "free water surface" is normally considered to be in equilibrium with the atmosphere or a surface at atmospheric pressure, and is usually assumed to be a limiting surface or boundary of the flow region. Muskat(6) defines a free surface as a "streamline along which the pressure is uniform." If we accept Muskat's definition (assuming atmospheric pressure along the free water surface) then the occurence of a free water surface in groundwater flow problems is more or less fortuitous since streamlines do not necessarily coincide with equipressural surfaces. Also the flow system is not limited by the "free water surface" since considerable amounts of flow can occur in the capillary zone lying above the water table. The water table simply represents an equipressural surface within the interior of the flow continuum and in general is not a stream surface (Luthin and Day, 4).

The importance of flow in the capillary zone is of course dependent on the relationship between the quantity of flow in the capillary zone as related to the flow in the groundwater zone or saturated zone lying below the water table. Recently Luthin and Day(4) have measured the lateral flow above a sloping water table and for the sand used in their experiment where the flow section below the water table was of the order of 30 cm thick, about half of the total flow was above the water table in the capillary zone. However for a

4. "The Use of Combined Electrical and Membrane Analogies to Investigate Unconfined Flow into Wells," by Chong Hung Zee, Ph.D. Dissertation, Utah State Agricultural College, Logan, Utah, 1952.
5. Asst. Prof. of Irrig., Univ. of California College of Agriculture, Davis, Calif.

groundwater zone 50 feet thick the contribution of the capillary zone above it would be less than 2 per cent of the total flow indicating that the authors were correct in ignoring the capillary zone in their analysis.

Laplace's equation is not valid for flow in the capillary region and any analysis of the total flow continuum depends on a solution of the equation

$$\text{div } (K\nabla\phi) = 0$$

where K (the permeability) is a function of the soil moisture tension. The relationship between K and the soil moisture tension may be determined experimentally although Childs and Colis-George(1) have proposed a method of calculating it from the soil moisture characteristic (a plot of soil moisture content vs. tension).

While the assumption of a "free water surface" may be justified in problems of well hydrology where the flow region below the water table is very large compared to capillary zone lying above the water table, it is doubtful if the concept can be applied with accuracy to certain problems of agricultural hydrology, highway drainage, and other flow problems involving thin flow regions below the water table.

The existence of a seepage surface at the well boundary has been adequately treated by the authors as well as others including Hansen(3) but an additional comment might be added. As has been pointed out by these authors there still seems to be some question in many minds as to the reason for the existence of a seepage surface. The usual reason given is that it must exist since if we assume the lack of a seepage surface then we have the impossible condition of intersecting streamlines with infinite velocities resulting. The reasonableness of having a seepage surface becomes apparent when we consider the condition necessary for water to enter a well. For water to pass as a liquid from a porous medium into the atmosphere the only requirement is that the pressure of the water in the porous media be equal to or greater than atmospheric. [Cf. Richards (71)] Such a condition is most certainly met in the situation of ground water flow toward a well.

In a homogenous soil mass of uniform permeability the length of the seepage surface is independent of the soil permeability. Such uniform soil conditions are seldom encountered in practice and usually the well penetrates a more permeable stratum. The greater the ratio of the permeability of the penetrated stratum to the permeability of the overburden the smaller will be the seepage surface. This conclusion can be inferred from the results of Luthin and Scott(5) who analyzed the steady state flow towards a well penetrating an aquifer having a permeability 100 times that of the overburden. The distribution of hydraulic head indicates that the water moves vertically out of the overburden to aquifer and then laterally to the well. It seems reasonable to infer that the seepage surface in this case would be rather small since water is passing from a layer of lower permeability to a layer of higher permeability [Cf. Day and Luthin (2)].

REFERENCES

1. Childs, E. C. and N. Colis-George. The permeability of porous materials. Proc. Royal Soc. America, 201:392-495, 1950.

2. Day, P. R. and J. N. Luthin. Pressure distribution in layered soils during continuous water flow. Soil Science Soc. of Amer. Proc. 17:87-91, 1953.

3. Hansen, V. E. Unconfined ground-water flow to multiple wells. Proc., Amer. Soc. of Civil Engr., V. 78, Sep. No. 142, 1952.

4. Luthin, J. N. and P. R. Day. Lateral flow above a sloping water table. Soil Science Soc. of Amer. Proc., 19:406-410, 1955.

5. Luthin, J. N. and V. H. Scott. Numerical analysis of flow through aquifers toward wells. Agr. Engr. 33:279-282, 1952.

6. Muskat, M. The flow of homogeneous fluids through porous media. McGraw-Hill Book Co. 1937.

7. Richards, L. A. Laws of soil moisture. Trans. Amer. Geophys. Union., 31:750-756, 1950.

CHIA-SHUN YIH.[1]—The authors are to be congratulated for having contributed so extensively to well hydraulics. It is, however, desirable to emphasize that the "membrane analogy" really does not exist for unconfined wells in the exact sense. For in Eq. (6) of the authors' paper, the second partial derivative of the piezometric head h with respect to the elevation z is not equal to zero for unconfined wells. It is true that on the free surface h is equal to z, but the equality of h and z is not maintained in the interior of the flow, and the error may not be small when the draw-down is not negligible compared with the asymptotic depth of the saturated layer. It is precisely in view of this that the consistency of the authors' data with those of previous investigators—particularly with those obtained by relaxation—is heartening. This consistency seems to indicate the general reliability of the authors' results and establishes a posteriori the fact that in spite of the lack of a rigorous membrane analogy, an approximate one nevertheless exists, the use of which has made the authors' extensive data possible.

Research workers in well hydraulics would render a great service to the profession if they would undertake the task of finding the exact solutions for a few well chosen cases, with a view to providing additional checks to the authors' results, especially in the regions where only their own data exist. This would finally and definitely establish the validity of the authors' extensive results covering a wide range of practical interest. On the other hand, the authors could make an additional contribution to well hydraulics if they would apply their technique to the treatment of partially penetrating wells or of the interference of wells.

1. Associate Prof., Iowa Inst. of Hydr. Research, Iowa City, Iowa.

Discussion of
"THICK RECTANGULAR PLATES ON AN ELASTIC FOUNDATION"

by Daniel Frederick
(Proc. Paper 818)

HAROLD G. LORSCH,[1] A.M. ASCE.—Dr. Frederick's paper is an excellent presentation of an application of the Reissner theory of thick plates. The writer fears, however, that the graphs presented might give a distorted picture of the numerical errors of the classical theory as compared to the more exact Reissner theory used in the paper.

Figures 4 and 5 show the results for values of $(kh^4/D) = 1$. The author states that this value was chosen for convenience. Unfortunately, this value does not correspond to usual practical problems. For, using a lean concrete plate ($E = 2000$ ksi, $\nu = 0.2$) and good soil ($k = 0.75$ kips per cubic inch) the thickness of the plate corresponding to $(kh^4/D) = 1$ is almost twenty feet. Needless to say that one would expect large shear effects in a plate of that thickness. For better concrete and/or softer soil the corresponding plate thickness increases.

For a steel plate ($E = 30{,}000$ ksi, $\nu = 0.3$) on a thin concrete block ($E = 2000$ ksi, $t = 1' = 0''$, hence $k = 200$ kips per cubic inch) the plate thickness for $(kh^4/D) = 1$ must be 13.75 inches, a very unusual value.

The writer feels that the reduction in bending stress of 55% (line 2, page 818-12 of the paper) should be viewed in the light of the above numerical calculations. Plates arising in civil engineering have (kh^2/D) ratios from 1/20 to 1/1000; it would indeed be interesting, if the author presented comparisons between the classical and the Reissner theory for that range. The writer expects the two methods to give nearly identical results for those cases.

None of these remarks are designed to detract from the fundamental approach used in the paper. They should merely reassure those engineers who might otherwise be inclined to disregard entirely the classical plate theory on account of the large errors shown in this paper.

1. Asst. Prof. of Civ. Eng., The City College, New York, N. Y.